A novel $K_3(Y_{0.88}Yb_{0.10}Er_{0.02})Si_2O_7$ silicate phosphor for multi-mode thermometry of high sensitivity through up-conversion luminescence

Jiantong Wang,[a] Bowen Wang,[a] Yuhan Teng,[a] Changshuai Gong,[a] Xuyan Xue,[a] Xuejiao Wang,[a*] Ji-Guang Li[b*]

[a]College of Chemistry and Materials Engineering, Bohai University, Jinzhou, Liaoning 121007, China

[b]Research Center for Functional Materials, National Institute for Materials Science, Tsukuba, Ibaraki 305-0044, Japan

*Corresponding author

Dr. Xuejiao Wang
Bohai University
Jianzhou, China
Tel: +86-416-3400708
E-mail: wangxuejiao@bhu.edu.cn

Dr. Ji-Guang Li
National Institute for Materials Science
Ibaraki, Japan
Tel: +81-29-860-4394
E-mail: li.jiguang@nims.go.jp

Abstract

Non-contract optical thermometry shows great advantages for temperature measurement in harsh environments, and it is highly desired to develop novel and high-performance systems. In this work, a novel $K_3(Y_{0.88}Yb_{0.10}Er_{0.02})Si_2O_7$ phosphor was synthesized *via* solid-state reaction, and its up-conversion luminescence and optical thermometric performance were systematically investigated. Under 980 nm excitation, the $K_3(Y_{0.88}Yb_{0.10}Er_{0.02})Si_2O_7$ phosphor showed a strong green UC emission through a three photon process. The phosphor was found well capable of sensing temperature *via* the multi-modes of fluorescence intensity ratio (FIR) of thermally/non-thermally coupled energy levels and fluorescence lifetime (FL). The maximum absolute (S_A) and relative (S_R) sensitivities are $S_A = 156\times10^{-4}$ K^{-1} (I_{531}/I_{555}, 298 K) and $S_R = 1.80\%$ K^{-1} (I_{519}/I_{555}, 298 K) *via* the FIR mode, and are $S_A = 661\times10^{-4}$ K^{-1} (548 K) and $S_R = 9.77\%$ K^{-1} (298 K) *via* the FL mode, which are higher than those of most previous studies.

Keywords: up-conversion; silicate; optical thermometry; rare earth luminescence

1. Introduction

Silicate compounds are an important phosphor family, which have aroused great research interests [1-9]. Phosphors based on silicates have good thermal and chemical stability and are widely used in cathode-ray luminescence and photoluminescence. Silicates include normal silicate, partial silicate, pyrosilicate, and other different systems. By controlling the ratio of chemical reagents and experimental conditions, different silicate phosphors can be obtained, such as $Ba_2La_8(SiO_4)_6O_2$: Eu^{2+} [2], $MgGd_4Si_3O_{13}$: Ce^{3+}, Mn^{2+} [3], $Mg_2Y_2Al_2Si_2O_{12}$: Tb^{3+}, Eu^{3+}, Tm^{3+} [4], $K_3ScSi_2O_7$: Eu^{2+} [5], etc. Silicates are an important choice for luminescence because of their significant absorption of ultraviolet (UV)/near-UV/blue light and low cost. At the same time, silicate-based phosphors have good physical properties, such as oxidation resistance, moisture resistance, and no interaction with the packaging resin [2,4,8,9]. The $[SiO_4]^{4-}$ unit, as the basic building block of silicates, can form relatively complicated crystal structures, which usually contain various complex anionic groups by different joining methods, forming islands, rings, chains, or layered structures [5,6,9]. Among the silicates, $A_3RESi_2O_7$ (A = Na, K; RE = Y, Gd, Lu), especially the $K_3RESi_2O_7$, has aroused intense research interests and various experiments have been carried out for the system [5,6,10-19]. It is found that different emissions, such as near-infrared emission [5,6], white emission [10], and near-ultraviolet emission [11], can be realized by adjusting the RE site.

However, the up-conversion (UC) luminescence of this $K_3RESi_2O_7$ system has not been reported up to date to the best of our knowledge. One of the reasons is that the compound is typically synthesized by the traditional solid-phase method, which, although effective for phosphor selection and synthesis, would produce micron-sized

large particles. It is difficult to obtain phosphors of nanometer size by this method, which greatly limits the application of UC phosphors of this system in the fields of biomarkers and anti-counterfeiting. Another reason is that the research interests of UC system are mainly on fluoride with low phonon energy, which would produce high UC efficiency [20-22]. However, fluoride is toxic, and its toxicity is related to its ability to dissociate fluorine ions.

Recently, the UC phosphors activated by Yb^{3+}-Er^{3+} pair are finding promising application as non-contact thermometers [7,20-23]. The intensity ratio of the 520 nm ($^2H_{11/2}\rightarrow{}^4I_{15/2}$) and 550 nm ($^4S_{3/2}\rightarrow{}^4I_{15/2}$) green luminescence Er^{3+} ion is very sensitive to temperature [24]. The temperature change will cause the obvious change in the ratio of these two branches, and the temperature can be determined by the branch ratio. Such application needs high thermal stability phosphors and doesn't require the phosphor particles to be nanosized. In previous studies, common UC phosphors usually use halogen-containing compounds as substrate [20-22], and Yb^{3+}/Er^{3+} co-doped $NaYF_4$($NaYF_4$: Yb^{3+}/Er^{3+}) is the most common UC material with the highest luminous efficiency. However, halogen-containing compounds need irritating and frequently toxic chemicals in the process of their synthesis. Therefore, various researches have been conducted to explore novel systems using the solid-state method [7,25-27]. In view of the outstanding down-conversion photoluminescence and thermal stability of $K_3YSi_2O_7$-based phosphors [10,13,14], we consider $K_3YSi_2O_7$ to be a promising host for UC luminescence. Thus, the typical ion pair of Yb^{3+}-Er^{3+} was doped into $K_3YSi_2O_7$ in this work, and the resulted phosphor was shown to be capable of multi-mode temperature measurement with high sensitivity through UC luminescence.

2. Experimental section

2.1 Reagents and synthesis

The rare earth sources for the synthesis were oxides (Y_2O_3, Yb_2O_3, Er_2O_3, 99.99% pure) bought from Huizhou Ruier Rare Chemical Hi-Tech Co. Ltd., Huizhou, China. The other reagents of K_2CO_3 (99.9% pure) and SiO_2 (99.99% pure) were purchased from Aladdin Industrial Corporation (Shanghai, China) and were used without further purification. $K_3(Y_{0.88}Yb_{0.10}Er_{0.02})Si_2O_7$ phosphors were synthesized by the conventional high-temperature solid-state method, where the contents of Yb and Er were taken as the optimal values of other UC systems [28,29]. The raw materials were weighed according to stoichiometric ratio, ground in agate mortar with alcohol for 20 minutes, mixed evenly, and then transferred to a corundum crucible. Finally, the mixture was heated at 1350 ℃ in a muffle furnace for 6 h in air, with a heating rate of 5 ℃/min before 800 ℃ and 3 ℃/min for 800-1350 ℃.

2.2 Characterization

The crystalline phases of the samples were identified by an X-ray diffractometer (XRD; Model Ultima IV, Rigaku, Tokyo, Japan) with Cu-K_α (λ = 0.15406 nm) radiation *via* the step-scan mode, with a step size of 0.01° and an accumulation time of 2 s in 2θ = 5-120^o range. Temperature-dependent UC spectra (RT-548 K) were measured using an FLS 1000 fluorospectrophotometer (Edinburgh Instruments Ltd., Herrsching am Ammersee, Britain), using a 980 nm continuous wavelength laser (2 W, Model MDL-III-980-2W-18050833) for excitation and a TAP-02 accessory for temperature control. The fluorescence decay kinetics of the main UC emissions were measured with the lifetime testing unit of the FLS 1000 equipment.

3. Results and discussion

3.1 Synthesis and visible-near-infrared luminescence of $K_3(Y_{0.88}Yb_{0.10}Er_{0.02})Si_2O_7$

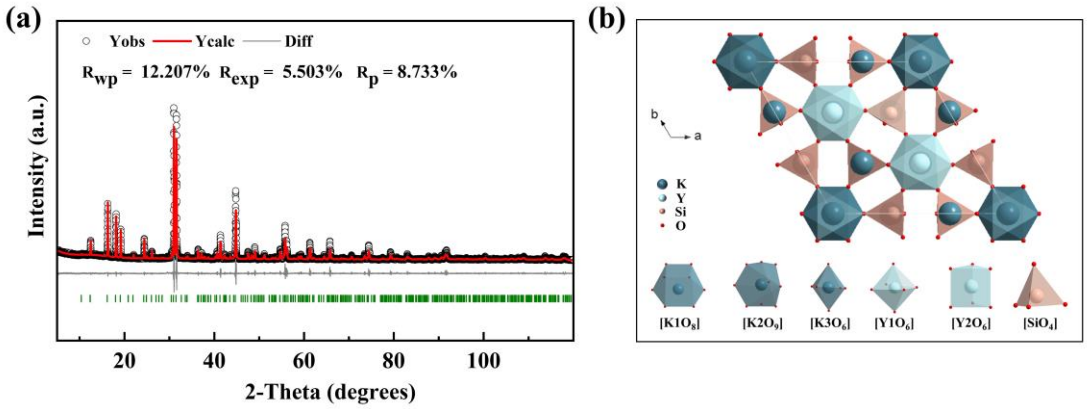

Figure 1 (a) Rietveld refinement for the $K_3(Y_{0.88}Yb_{0.10}Er_{0.02})Si_2O_7$ phosphor, where the observed and calculated patterns, the difference, and the positions of Bragg reflections are in black, red, gray and green, respectively, (b) crystal structure of $K_3YSi_2O_7$, together with the coordination environment of the cation.

Figure 1(a) shows the Rietveld refinement results of the obtained $K_3(Y_{0.88}Yb_{0.10}Er_{0.02})Si_2O_7$ phosphor. The refinement yielded stable results and acceptable reliability factors, which indicate that the product is of high purity. The detailed refinement results are shown in Table 1 and Table 2. According to Loye et al., $K_3YSi_2O_7$ may have two polymorphs, namely $K_3YSi_2O_7$(1) and $K_3YSi_2O_7$(2), which belong to *P*63/*mmc* and *P*63/*mcm* space groups, respectively [10]. In this work, we obtained $K_3YSi_2O_7$(2) with the second space group. Figure 1(b) are the crystal structure observed from the *c*-axis and the coordination polyhedra of cations for $K_3YSi_2O_7$(2). The compound $K_3YSi_2O_7$(2) (ICSD 430538) has a hexagonal structure with lattice constants a = 9.8450 Å, c = 14.3236 Å. c/a = 1.4549. It consists of SiO_4, $K1O_8$, $K2O_9$, $K3O_6$, $Y1O_6$, and $Y2O_6$ units connected by shared oxygen atoms. $K_3YSi_2O_7$(2) has two distinct yttrium sites, one distinct silicon site, three distinct potassium sites, and three distinct oxygen sites [13]. The two yttrium sites are

independent of each other and are located in a hexagonal coordination environment. Y(1) is located in a regular hexagonal octahedron, and Y(2) is located in a hexagonal trigonal prism. $Y1O_6$ is connected to SiO_4 by oxygen atoms at shared vertices, and SiO_4 forms the Si_2O_7 pyrosilicate structure by bridging oxygen atoms at shared vertices. The coordination numbers of K(1), K(2), and K(3) are 8, 9, and 6 respectively. The K(1) site is aligned with Si along the *c*-axis, the K(2) site is aligned with Y(1) along the *c*-axis, and the K(3) site is aligned with Y(2) along the *c*-axis. In addition, it can be seen that the lattice parameters and cell volume of the Yb^{3+}-Er^{3+} co-doped sample is smaller than those of the pure host as also shown in Table S1. This conforms well to the fact that Er^{3+} (R = 0.890, CN = 6) and Yb^{3+} (R = 0.868, CN = 6) have smaller ionic radii than Y^{3+} (R = 0.900, CN = 6) [30], and indicates successful incorporation of the dopant ions to form solid solution.

Table 1 Experimental parameters of powder XRD and refined crystallographic data for $K_3(Y_{0.88}Yb_{0.10}Er_{0.02})Si_2O_7$.

Chemical Formula	$K_3(Y_{0.88}Yb_{0.10}Er_{0.02})Si_2O_7$
Diffractometer	X'Pert Pro, PANalytical
Radiation type	Cu Kα, λ = 1.54060 Å
2θ interval (°)	5.00-120.00
Step size of 2θ (°)	0.01
Space group	*P*63/*mcm* (193)
Z	6
a (Å)	9.8419(2)
b (Å)	9.8419(2)
c (Å)	14.3032(4)
V (Å^3)	1199.85(6)
Number of structure parameters	27
Number of profile parameters	35
[b] R_p (%)	8.73
[c] R_{wp} (%)	12.21
[d] S	2.22

[b] $R_P = \sum |y_i - y_{C,i}| / \sum y_i$; [c] $R_{wp} = \left[\sum w_i |y_i - Y_{C,i}|^2 / \sum w_i y_i^2\right]^{\frac{1}{2}}$; [d] $S = R_{wp} / R_{exp}$

Table 2 Wyckoff positions, atomic coordinates, and occupancies of $K_3(Y_{0.88}Yb_{0.10}Er_{0.02})Si_2O_7$.

Atom	Site	*x*	*y*	*z*	Occupancy
Y1	4	0.3333	0.6667	0	0.89
Yb1	4	0.3333	0.6667	0	0.10
Er1	4	0.3333	0.6667	0	0.01
Y2	2	0	0	0.25	0.91
Yb2	2	0	0	0.25	0.08
Er2	2	0	0	0.25	0.01
K1	12	0.32798	0	0.09211	1
K2	4	0.3333	0.6667	0.25	1
K3	2	0	0	0	1
Si1	12	0.65938	0	0.14315	1
O1	24	0.67437	0.15042	0.09402	1
O2	12	0.81453	0	0.14696	1
O3	6	0.59540	0	0.25	1

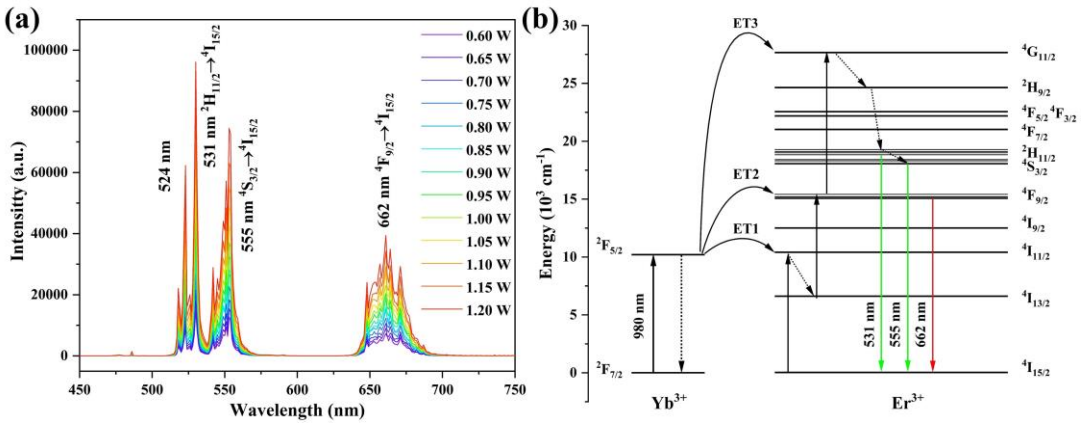

Figure 2 (a) Emission spectra of $K_3(Y_{0.88}Yb_{0.10}Er_{0.02})Si_2O_7$ phosphor in the visible light range (450-750 nm) at different excitation powers of 980 nm laser. (b) The proposed up-conversion mechanism, where ET means energy transfer.

The UC spectra of $K_3(Y_{0.88}Yb_{0.10}Er_{0.02})Si_2O_7$ excited at different powers (0.60-1.20 W) are shown in Figure 2. The emission spectra consist of green emissions in the range of 510-575 nm and red emissions in the 630-700 nm region. The emission peaks at 531 nm and 555 nm belong to the transitions from $^2H_{11/2}$ and $^4S_{3/2}$ excited states to $^4I_{15/2}$ ground state of Er^{3+}, respectively, while the red emission near 670 nm is generated by the transition from $^4F_{9/2}$ to $^4I_{15/2}$. The number of photons (*n*) required to excite the ground state electron to the emission state can be estimated by the $I_{em} \propto P^n$ equation [29]. The logarithmic curves of I_{em} and P^n at different powers are shown in

Figure S1 for the $K_3(Y_{0.88}Yb_{0.10}Er_{0.02})Si_2O_7$ phosphor. The slope of the graph is the number of photons required (*n*). The slope of the curve (*n* value) in Figure S1 is about 3 for green emission and 2 for red emission, indicating that the observed UC luminescence is essentially caused by three (green) and two-photon (red) mechanism. The energy level diagram of Yb^{3+} and Er^{3+} in $K_3(Y_{0.88}Yb_{0.10}Er_{0.02})Si_2O_7$ and the emission mechanism of UC are shown in Figure 2b. The three-photon process corresponding to green emission is as follows. Under the excitation of 980 nm laser, the electrons of Yb^{3+} are excited to the $^2F_{5/2}$ level, from which energy transfer to the neighboring Er^{3+} would take place. The energy absorption of Er^{3+} ion excites electrons from the ground state $^4I_{15/2}$ to the excited state $^4I_{11/2}$ (ET1), followed by non-radiative relaxation (NR) to the $^4I_{13/2}$ level. With the energy of the second excitation photon, the Er^{3+} electrons were raised to the $^4F_{9/2}$ level (ET2). Subsequently, the Er^{3+} electrons were eventually excited to the $^4G_{11/2}$ level by ET3 and then relax to $^2H_{11/2}$ through non-radiative transition. Backing jumping of the $^2H_{11/2}$ electrons to the ground state then produced the green light. The whole process can also be expressed as follows [31,32]:

(1) $^2F_{7/2}$ (Yb^{3+}) + 980 nm photon → $^2F_{5/2}$ (Yb^{3+})

(2) $^2F_{5/2}$ (Yb^{3+}) + $^4I_{15/2}$ (Er^{3+}) → $^2F_{7/2}$ (Yb^{3+}) + $^4I_{11/2}$ (Er^{3+}) (ET1)

(3) $^4I_{11/2}$ (Er^{3+}) → $^4I_{13/2}$ (Er^{3+}) (NR)

(4) $^2F_{5/2}$ (Yb^{3+}) + $^4I_{13/2}$ (Er^{3+}) → $^2F_{7/2}$ (Yb^{3+}) + $^4F_{9/2}$ (Er^{3+}) (ET2)

(5) $^2F_{5/2}$ (Yb^{3+}) + $^4F_{9/2}$ (Er^{3+}) → $^2F_{7/2}$ (Yb^{3+}) + $^4G_{11/2}$ (Er^{3+}) (ET3)

(6) $^4G_{11/2}$ (Er^{3+}) → $^2H_{9/2}$ (Er^{3+}) → $^2H_{11/2}$ (NR)

(7) $^{2}H_{11/2}$ (Er^{3+}) → $^{4}I_{15/2}$ (Er^{3+}) + photons (531 nm)

For the emission peaks at 555 nm, the first six processes are the same as those of the 531 nm emission. The difference is that the electrons at the $^{2}H_{11/2}$ energy level of Er^{3+} relax to the $^{4}S_{3/2}$ by NR, and the occurrence of $^{4}S_{3/2}$ (Er^{3+})→$^{4}I_{15/2}$ (Er^{3+}) and transitions emit photons at 555 nm. For the red emission located at 662 nm, its two-photon process is that, after the first four transition steps, the electron at the $^{4}F_{9/2}$ energy level transits to the ground state and emits a photon.

It can be seen that for $K_3(Y_{0.88}Yb_{0.10}Er_{0.02})Si_2O_7$ phosphor, the increasing excitation power does not change the shape and position of the emission peak, but the intensity of the emission gradually increased.

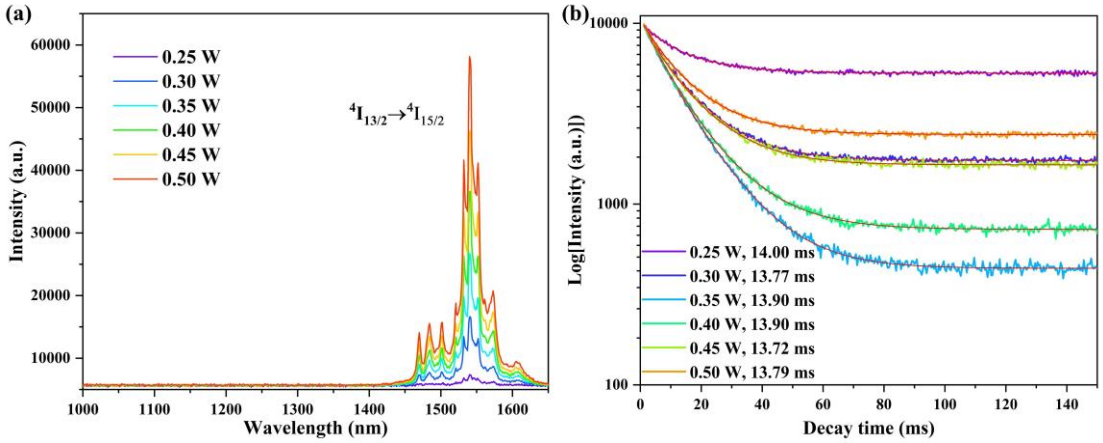

Figure 3 (a) Emission spectra of $K_3(Y_{0.88}Yb_{0.10}Er_{0.02})Si_2O_7$ phosphor in the near-infrared range (1000-1600 nm) at different excitation powers of 980 nm laser. (b) Fluorescence decay kinetics of the 1542 nm emission at different excitation powers (0.25-0.50 W), where the numbers following the power are the average lifetimes.

The emission spectra of $K_3(Y_{0.88}Yb_{0.10}Er_{0.02})Si_2O_7$ in the near-infrared region at different powers are shown in Figure 3a. The strongest peak is at 1542 nm, which corresponds to the $^{4}I_{13/2}$→$^{4}I_{15/2}$ transition of Er^{3+} [33]. It can be seen that the sample has a strong broadband emission in the near-infrared region. The Stark splitting of the NIR emission is evident because of the splitting of the 4*f* level of Er^{3+} ions due to the

action of the crystal field. Figure 3b shows the decay kinetics of the 1542 nm emission, where it was found that all the curves are well fitted using the double-order exponential equation [34,35]:

$$I(t) = A_1 exp(-t/\tau_1) + A_2 exp(-t/\tau_2) \qquad (1)$$

where A_1 and A_2 are constants, t is decay time, I(t) is luminescence intensity at time t, τ_1, and τ_2 are the fast and slow components of lifetime respectively. The average lifetime (τ) can be obtained by the following equation [34,35]:

$$\tau = (A_1\tau_1^2 + A_2\tau_2^2)/(A_1\tau_1 + A_2\tau_2) \qquad (2)$$

The derived τ and A values and the chi-square factor (χ^2) of fittings are summarized in Table S2. The 1542 nm emissions at different powers show similar average lifetime of around 14 ms.

3.2 Multi-mode thermometric properties of $K_3(Y_{0.88}Yb_{0.10}Er_{0.02})Si_2O_7$

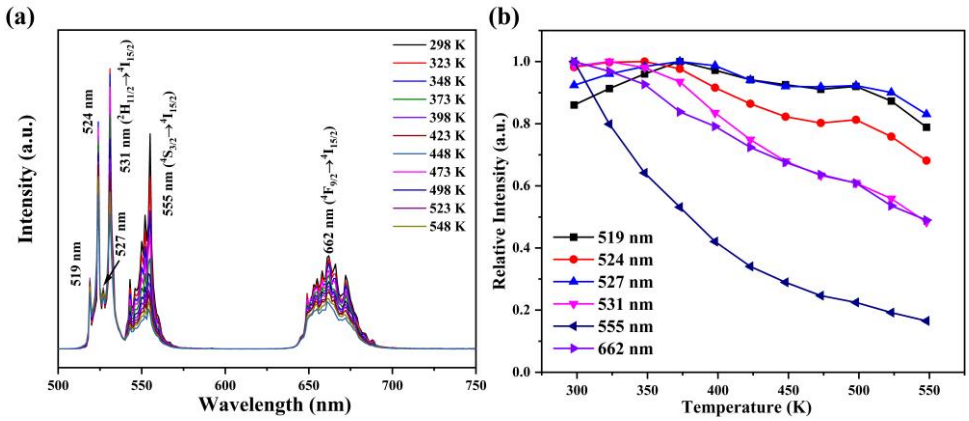

Figure 4 (a) Emission spectra of $K_3(Y_{0.88}Yb_{0.10}Er_{0.02})Si_2O_7$ phosphor excited by 980 nm laser (0.5 W) at different temperatures (RT-548 K). (b) Relative emission intensity for different transitions as a function of the measured temperature.

In practical applications, especially in the field of temperature measurement, the relationship between luminescence intensity and temperature is of great importance. Therefore, we tested the PL spectra of $K_3(Y_{0.88}Yb_{0.10}Er_{0.02})Si_2O_7$ in the temperature range of 298-548 K, as shown in Figure 4a. As can be seen from Figure 4a, the

luminescence intensity of the sample decreases gradually with increasing temperature and the specific CIE coordinates are given in Figure S2 and Table S3. As can be seen from Figure S2, the color coordinates of $K_3(Y_{0.88}Yb_{0.10}Er_{0.02})Si_2O_7$ did not shift much with increasing temperatures. Figure 4b shows the relationship between normalized emission intensity and temperature. The results show that the green emission intensity of 519/527 nm ($^2H_{11/2}\rightarrow{}^4I_{15/2}$) increases with increasing temperature, reaching the maximum value at 373 K and maintaining 97.2% and 98.7% of the maximum intensity at 423 K, respectively. At the highest measurement temperature of 548 K, 78.9% and 83.0% of the maximum emission intensity can still be retained, respectively. For 555 nm ($^4S_{3/2}\rightarrow{}^4I_{15/2}$) emission, the intensity decreases obviously with increasing temperature. The intensity loss rates of $^2H_{11/2}\rightarrow{}^4I_{15/2}$ and $^4S_{3/2}\rightarrow{}^4I_{15/2}$ are different with increasing temperature. This indicates that the prepared phosphor can sense temperature through the fluorescence intensity ratio (FIR) of the thermally coupled $^2H_{11/2}$ and $^4S_{3/2}$ levels and has potential application in the field of optical thermometry. The $^4F_{9/2}\rightarrow{}^4I_{15/2}$ (662 nm) emission also decreased monotonically with increasing temperature. Since $^2H_{11/2}$ and $^4S_{3/2}$ are thermally coupled energy levels (ΔE = 736 cm^{-1}), their population follows Boltzmann distribution. The FIR of the two different green emissions can be expressed as [36,37]:

$$\mathrm{FIR} = \frac{I_H}{I_S} = A \cdot \exp\left(-\frac{\Delta E}{k_B T}\right) + C \qquad (3)$$

where I_H and I_S represent the emission intensity of the $^2H_{11/2}\rightarrow{}^4I_{15/2}$ and $^4S_{3/2}\rightarrow{}^4I_{15/2}$ transitions; ΔE is the energy level gap between corresponding energy levels; k_B is Boltzmann constant; T is the absolute temperature; A and C are constants.

Equation (3) is used to fit the FIR relation with temperature of the two thermal coupled energy levels. The fitting curve is shown in Figure 5a, and the points in the figure are experimental data. It can be seen from the figure that as the temperature rises from 298 K to 548 K, The I_{531}/I_{555} ratios of $K_3(Y_{0.88}Yb_{0.10}Er_{0.02})Si_2O_7$ increase gradually. According to the Boltzmann distribution law, when the temperature increases, electrons are more easily pumped to the higher $^2H_{11/2}$ energy level to reach equilibrium. In addition, the probability of the non-radiative transition from $^4S_{3/2}$ to $^4I_{15/2}$ increases, so the emission at 555 nm is significantly weakened, thus increasing the ratios of I_{531}/I_{555}.

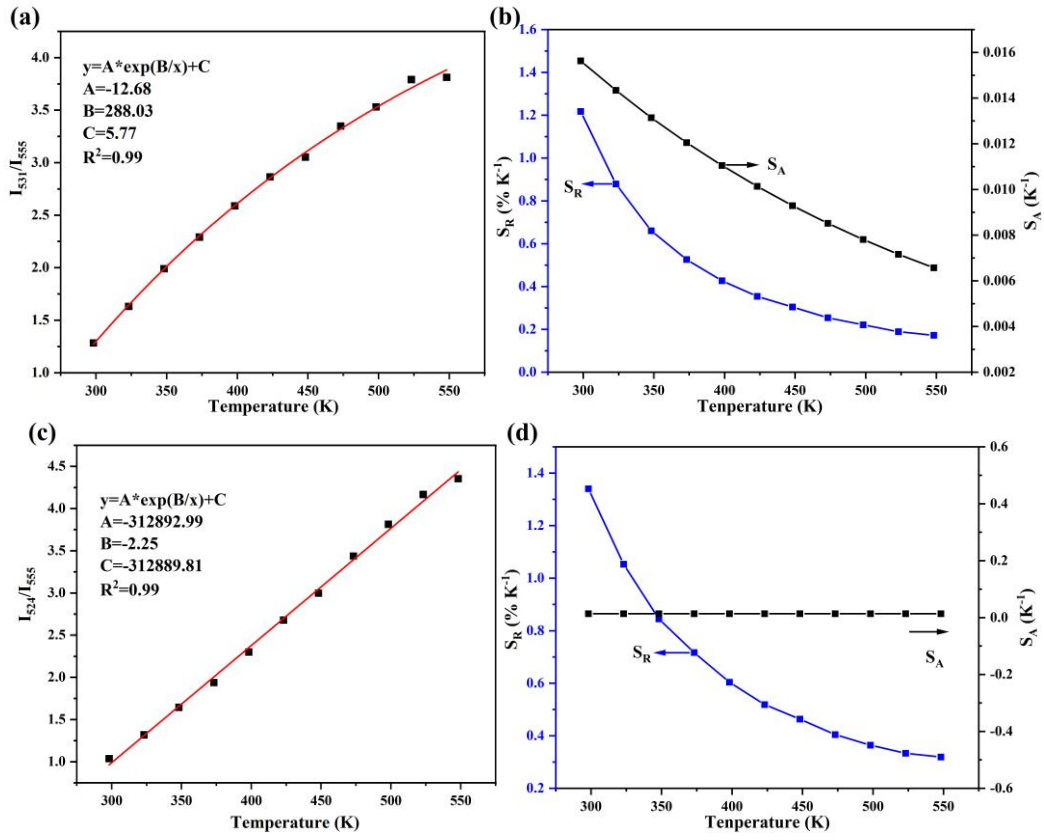

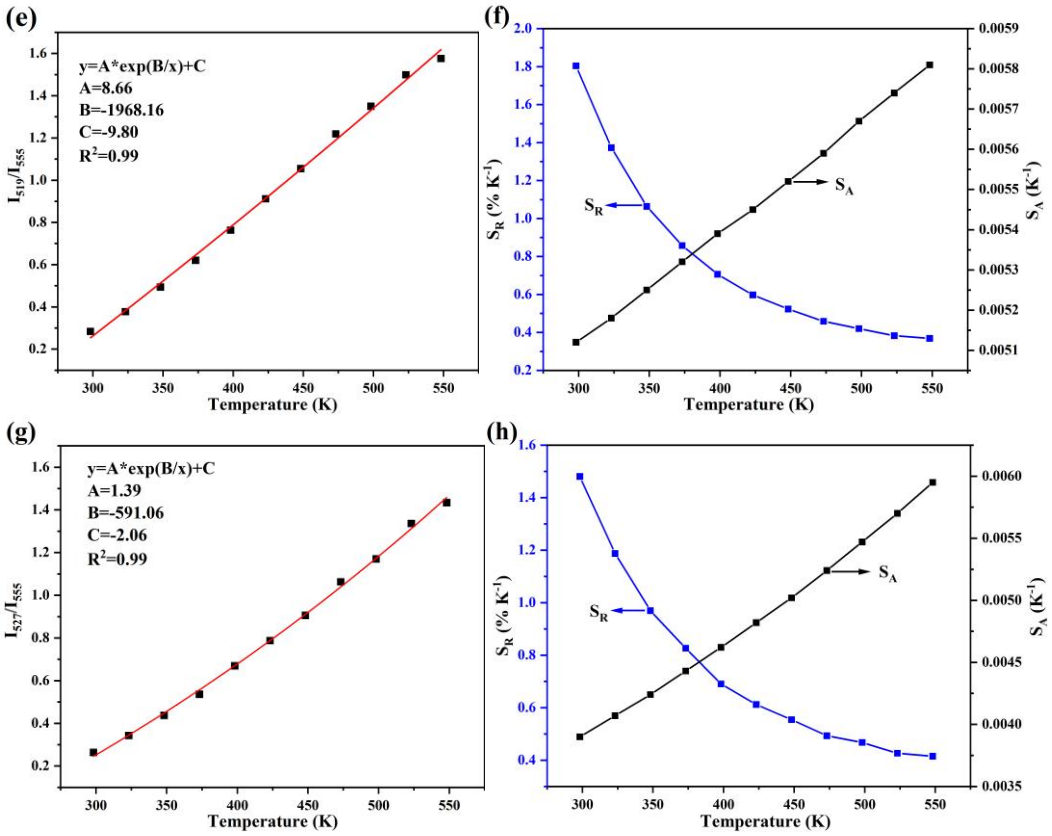

Figure 5 Different FIRs and their corresponding S_A and S_R values as a function of the measurement temperature for the $K_3(Y_{0.88}Yb_{0.10}Er_{0.02})Si_2O_7$ phosphor.

In addition, sensitivity S is an important index to evaluate the sensitivity of phosphors to temperature change, which can be expressed by absolute sensitivity S_A and relative sensitivity S_R. The calculation equations are as follows [37]:

$$S_A = \left|\frac{d(FIR)}{d(T)}\right| = (FIR - C) \times \frac{\Delta E}{k_B T^2} \qquad (4)$$

$$S_R = \left|\frac{d(FIR)}{d(T)}\frac{1}{FIR}\right| = \frac{FIR-C}{FIR} \times \frac{\Delta E}{k_B T^2} \qquad (5)$$

Equation (4) and Equation (5) were used to calculate S_A and S_R, respectively. As shown in Figure 5b, the maximum values of S_A and S_R corresponding to I_{531}/I_{555} are 156×10^{-4} K^{-1}(298 K) and 1.22% K^{-1}(298 K), respectively; while the maximum values of S_A and S_R corresponding to I_{519}/I_{555} are 58×10^{-4} K^{-1}(548 K) and 1.80% K^{-1}(298 K), respectively.

The energy difference (ΔE) of thermally coupled levels is generally between 200 ~ 2000 cm^{-1}. Compared with the traditional technology based on the FIR of thermally

coupled energy levels, the temperature measurement based on non-thermally coupled energy levels (NTCL) is not limited by the energy difference, and the number of energy level pairs is rich, which is beneficial to improve the accuracy of temperature measurement. We calculated the temperature sensitivity of the $K_3(Y_{0.88}Yb_{0.10}Er_{0.02})Si_2O_7$ phosphor. The temperature-dependent FIR of non-thermally coupled energy levels can be fitted by a polynomial function [38]:

$$FIR = \frac{I_{555}}{I_{662}} = A + BT + CT^2 + DT^3 \qquad (6)$$

where A, B, C, and D are constants. As shown in Figure 6a, the variation of the fluorescence intensity ratio FIR(I_{555}/I_{662}) of the non-thermally coupled energy levels with temperature can be well fitted by Equation (6), with R^2 = 0.99. In this case, the sensitivity of temperature sensing can be calculated with the following equation [38]:

$$S = \frac{d(FIR)}{dT} = B + 2CT + 3DT^2 \qquad (7)$$

The curve of sensitivity as a function of temperature is shown in Figure 6b, where the sensitivity reached a maximum value of 157×10^{-4} K^{-1} at 298 K.

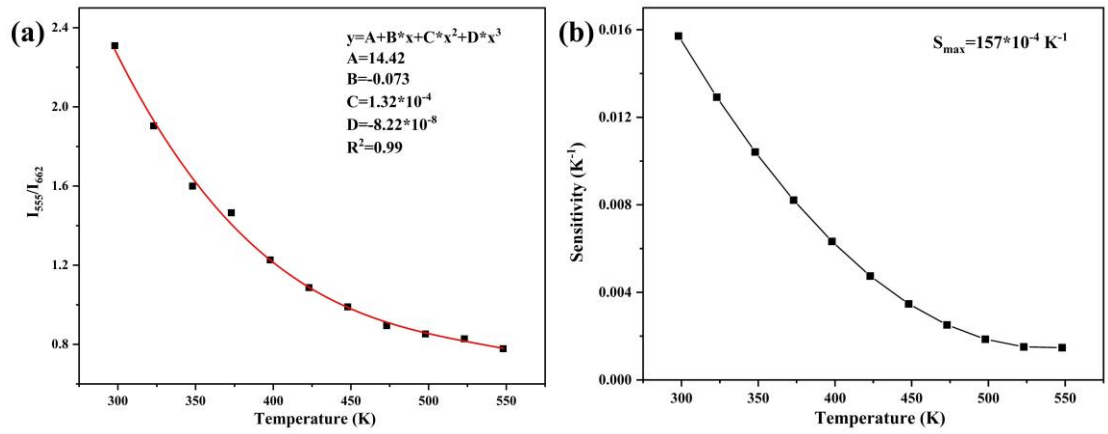

Figure 6 (a) The FIR of the 555 nm and 662 nm emission peaks of $K_3(Y_{0.88}Yb_{0.10}Er_{0.02})Si_2O_7$ as a function of temperature and (b) sensitivity as a function of temperature.

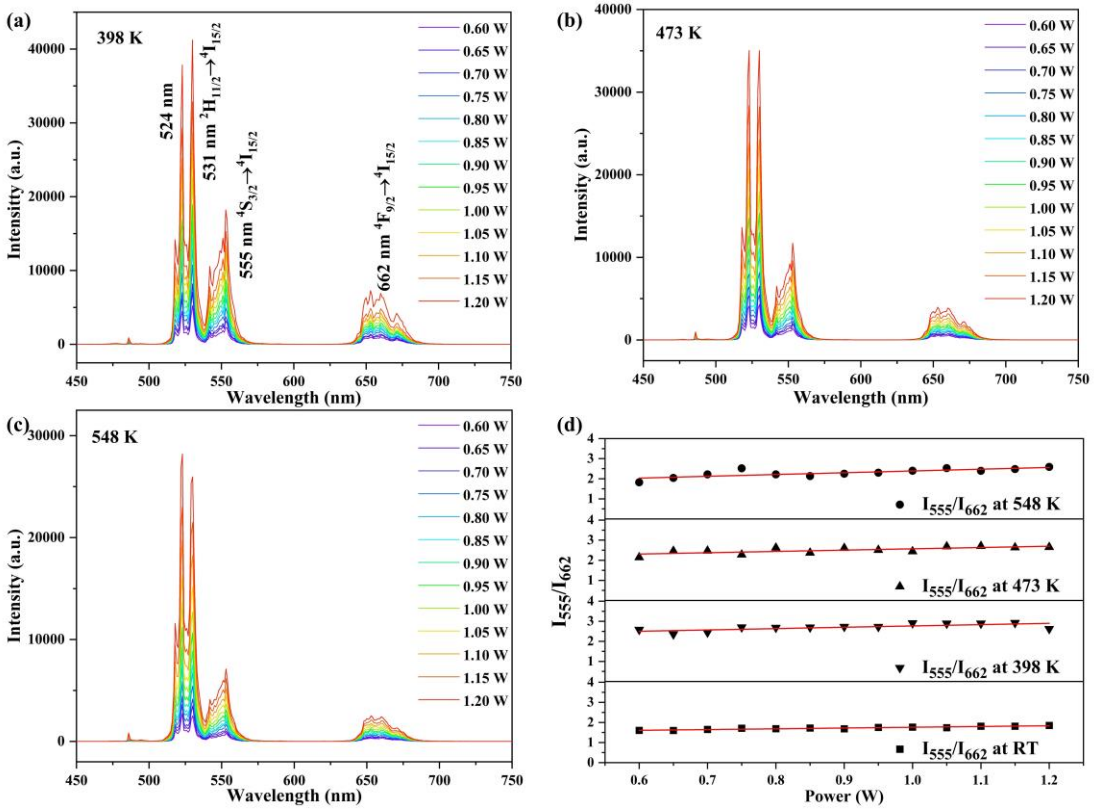

Figure 7 Emission spectra of $K_3(Y_{0.88}Yb_{0.10}Er_{0.02})Si_2O_7$ phosphor excited with different powers 980 nm laser at (a) 398 K, (b) 473 K, and (c) 548 K. (d) The variation trend of I_{555}/I_{662} with excitation power at different temperatures.

Although quite a number of references used Equation (6) for the FIR fitting of non-thermally coupled energy levels, the excitation power was not involved in the equation. Such fitting cannot reflect the influence of the excitation power on FIRs. In order to ensure the accuracy of the results, the power dependent emission spectra at different temperatures (398 K, 473 K, 548 K) were measured and the I_{555}/I_{662} FIR at different excitation powers was evaluated. As seen from the results shown in Figure 7, I_{555}/I_{662} FIR is stable under varying excitation power at different temperatures and, therefore, the influence of excitation power during the temperature-sensing calculation of the non-thermally coupled energy level can be excluded. The influence of excitation power on the other two FIRs were also checked and were shown in Figure S4. It was found that excitation power has a small influence on the FIRs

values.

Table 3 summarizes the S_A and S_R values of several typical phosphors with optical temperature sensing behavior. Through comparison, it was found that the maximum value of S_A and S_R obtained in this work are higher than these of most systems. Among them, the sensitivity values calculated based on non-thermally coupled energy levels are higher than those obtained by the thermally coupled energy levels. The results show that $K_3(Y_{0.88}Yb_{0.10}Er_{0.02})Si_2O_7$ phosphor has potential application value in optical temperature measurement.

Table 3. A summary of S_A and S_R values, and temperature sensing ranges for some typical temperature sensing phosphors.

Ion pair	Mode	Host	Range (K)	$S_A(K^{-1})\times10^{-4}$	$S_R(\%\ K^{-1})$	Ref
Yb^{3+}-Er^{3+}	FIR	KY_3F_{10}(Core-Only)	310-366	-	1.51 (310 K)	[20]
Yb^{3+}-Er^{3+}	FIR	KY_3F_{10}(Core-Shell)	300-365	-	1.24 (316 K)	[20]
$Yb^{3+}/Er^{3+}/Mn^{2+}$	FIR	$NaBiF_4$	298-473	55.9 (473 K)	1.22 (298 K)	[21]
Yb^{3+},Er^{3+}	FIR	$NaScF_4$	298-573	25.6 (548 K)	0.31	[22]
Yb^{3+},Er^{3+}	FIR	$NaScF_4$(EDTA)	298-573	32.8 (548 K)	0.41	[22]
Yb^{3+},Er^{3+}	FIR	$Na_2GdMg_2(VO_4)_3$	303-573	74.9 (479 K)	0.98 (303 K)	[23]
Er^{3+}	FIR	$GdTaO_4$	293-723	41 (475 K)	1.12 (298 K)	[24]
Yb^{3+},Er^{3+}	FIR	$Ba_5Y_8Zn_4O_{21}$	293-563	0.39 (563 K)	136 (293 K)	[25]
Er^{3+}	FIR	$LaGdO_3$	298-873	43 (554 K)	1.20 (298 K)	[26]
Bi^{3+}/Tb^{3+}	FIR	$LaNdO_4$	303-483	410	2.36	[27]
Bi^{3+}/Eu^{3+}	FIR	$LaNdO_4$	303-483	440	1.89	[27]
Bi^{3+}/Dy^{3+}	FIR	$LaNdO_4$	303-483	80	1.26	[27]
Bi^{3+}/Sm^{3+}	FIR	$LaNdO_4$	303-483	310	1.36	[27]
Yb^{3+}/Er^{3+}	FIR	Y_2O_3	323-573	196 (543 K)	-	[39]
Pr^{3+}	FL	La_2MgTiO_6	298-548	2.85	1.81 (473 K)	[40]
Sm^{2+}	FL	$SrBa_4O_7$	298-723	-	3.36 (500 K)	[41]
Eu^{2+}	FL	$Li_4ScCa(SiO_4)_2$	303-573	1470	15.0	[42]
Dy^{3+}/Mn^{4+}	FL	Li_2TiO_3/Y_2O_3	273-373	220 (308 K)	6.67 (339 K)	[43]
Yb^{3+},Er^{3+}	$FIR(I_{531}/I_{555})$	$K_3YSi_2O_7$	298-548	156 (298 K)	1.22 (298 K)	This work
Yb^{3+},Er^{3+}	$FIR(I_{527}/I_{555})$	$K_3YSi_2O_7$	298-548	59 (548 K)	1.48 (298 K)	This work
Yb^{3+},Er^{3+}	$FIR(I_{519}/I_{555})$	$K_3YSi_2O_7$	298-548	58 (548 K)	1.80 (298 K)	This work
Yb^{3+},Er^{3+}	$FIR(I_{524}/I_{555})$	$K_3YSi_2O_7$	298-548	139	1.34 (298 K)	This work
Yb^{3+},Er^{3+}	$FIR_{NTCL}(I_{555}/I_{662})$	$K_3YSi_2O_7$	298-548	157 (298 K)	-	This work
Yb^{3+},Er^{3+}	FL(531 nm)	$K_3YSi_2O_7$	323-548	661 (548 K)	9.77 (298 K)	This work

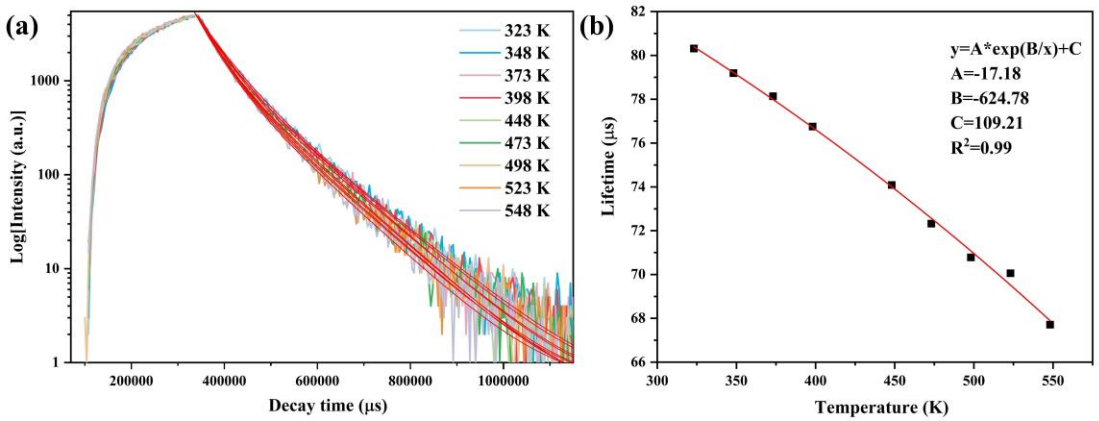

Figure 8 (a) Fluorescence decay kinetics of 531 nm emission at different temperatures (RT-548 K), and (b) the relationship of fluorescence lifetimes for 531 nm emission with measurement temperature (RT-548 K). The intensity in (a) is in logarithmic form.

Figure 8a shows the fluorescence decay curves for the 531 nm emission of $K_3(Y_{0.88}Yb_{0.10}Er_{0.02})Si_2O_7$ phosphor under 980 nm laser excitation at different temperatures. As shown in the figure, all the curves are well fitted using the double-order exponential Equation (1). Then, the average lifetime (τ) can be obtained by the following Equation (2). The derived lifetime of the 531 nm emission is shown in Figure 8b, where it is seen that the lifetime monotonously decreased from 80.31 μs (323 K) to 67.71 μs (548 K). The 531 nm emission at other temperatures showed a similar decay behavior and the derived τ and A values and the chi-square factor (χ^2) of fittings are summarized in Table S4. The χ^2 values for all the fittings are around 1, indicating the high quality of the fitting. It is noteworthy that the fluorescence lifetime of $K_3(Y_{0.88}Yb_{0.10}Er_{0.02})Si_2O_7$ decreases with increasing temperature, which can be attributed to increased non-radiative transitions in the matrix lattice. This trend is the same as that observed from the temperature-dependent emission intensity. As shown in Figure 8b, the lifetime of the 531 nm emission decreases exponentially with increasing temperature T, and can be expressed as τ_{531} = -17.18exp (-624.78/T) + 190.91.

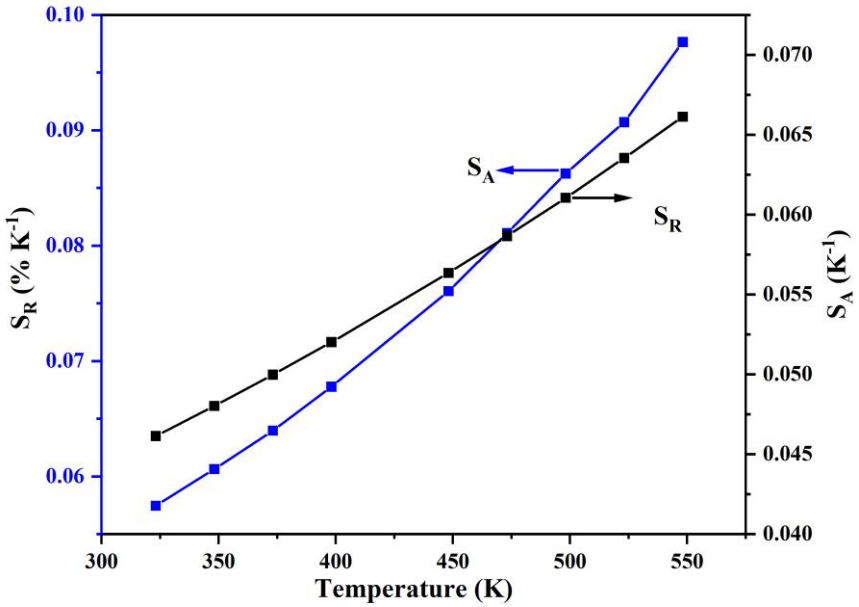

Figure 9 The relative sensitivity S_R and absolute sensitivity S_A based on the fluorescence lifetime of 531 nm emission for $K_3(Y_{0.88}Yb_{0.10}Er_{0.02})Si_2O_7$ phosphor.

Aside from those utilizing the FIR technology, a temperature sensing scheme based on fluorescence lifetime (FL) can also be realized with the thermal quenching characteristics of $K_3(Y_{0.88}Yb_{0.10}Er_{0.02})Si_2O_7$. Similar to the scheme based on FIR, the absolute sensitivity S_A and relative sensitivity S_R of FL based temperature sensing can be calculated by the following Equation [40,42-44]:

$$S_A = \left|\frac{d\tau}{dT}\right| \qquad (8)$$

$$S_R = \frac{1}{\tau}\left|\frac{d\tau}{dT}\right| \qquad (9)$$

As shown in Figure 9, the phosphor has maximum values were 661×10^{-4} K^{-1}(548 K) and 9.77% K^{-1}(548 K) for S_A and S_R, respectively. It can be seen from the figure that S_A and S_R both increase with increasing temperature. By comparing the S_R value based on the FL mode and the S_R value based on the FIR mode, it is obvious that the former is greater than the latter. Nevertheless, as shown in Table 3, the S_R values of both the FIR and FL modes obtained in this work are better than those of most previous studies.

Conclusions

A novel $K_3(Y_{0.88}Yb_{0.10}Er_{0.02})Si_2O_7$ silicate phosphor was prepared by solid reaction. The UC luminescence properties, UC mechanism as well as the performance of optical temperature sensing *via* multi-modes were systematically investigated. The main conclusions are as follows:

(1) The $K_3(Y_{0.88}Yb_{0.10}Er_{0.02})Si_2O_7$ new phosphor exhibits strong green luminescence through $^2H_{11/2}\rightarrow{}^4I_{15/2}$ transition (531 nm) under 980 nm excitation, which occurs through a three photon processes.

(2) $K_3(Y_{0.88}Yb_{0.10}Er_{0.02})Si_2O_7$ is well capable of temperature sensing *via* fluorescence intensity ratio (FIR) with thermally coupled/non-thermally coupled energy levels (TCL/NTCL) and fluorescence lifetime (FL). The maximum S_A and S_R values are $S_A = 156\times10^{-4}$ K^{-1} (I_{531}/I_{555}, 298 K) and $S_R = 1.80\%$ K^{-1} (I_{519}/I_{555}, 298 K) for the FIR mode, and are $S_A = 661\times10^{-4}$ K^{-1} (548 K) and $S_R = 9.77\%$ K^{-1} (298 K) for the FL mode.

Acknowledgements

This work is supported by Natural Science Foundation of Liaoning Province (Grant No. 2020-MS-286). The authors would like to thank Siqi Liu from Shiyanjia Lab (www.shiyanjia.com) for the XRD measurement.

References

[1] X. Ji, J. Zhang, Y. Li, S. Liao, X. Zhang, Z. Yang, Z. Wang, Z. Qiu, W. Zhou, L. Yu, S. Lian, Improving quantum efficiency and thermal stability in blue-emitting $Ba_{2-x}Sr_xSiO_4$: Ce^{3+} phosphor *via* solid solution, Chem. Mater. 30 (2018) 5137-5147.

https://doi.org/10.1021/acs.chemmater.8b01652.

[2] T. Sun, D. Liu, Y.G. Liu, X. Bu, H. Yu, J. Yang, C.A. Xie, J. Chen, A novel cyan-emitting phosphor $Ba_2La_8(SiO_4)_6O_2$: Eu^{2+} for full-spectrum white light-emitting diodes, Opt. Mater. 127 (2022) 1112287. https://doi.org/10.1016/j.optmat.2022.112287.

[3] A. Deng, Z. Wang, X. Zhou, W. Geng, $MgGd_4Si_3O_{13}$: Ce^{3+}, Mn^{2+}: A Dual-Excitation Temperature Sensor, ACS Omega. 7 (2022) 6481-6487. https://doi.org/10.1021/acsomega.1c04710.

[4] X. Huo, Z. Wang, C. Tao, N. Zhang, D. Wang, J. Zhao, Z. Yang, P. Li, Single-component white emitting phosphor $Mg_2Y_2Al_2Si_2O_{12}$: Tb^{3+}, Eu^{3+}, Tm^{3+} for white LEDs, J. Alloys Compd. 902 (2022) 163823. https://doi.org/10.1016/j.jallcom.2022.163823.

[5] Q. Zhang, X. Wang, Z. Tang, Y. Wang, A $K_3ScSi_2O_7$: Eu^{2+} based phosphor with broad-band NIR emission and robust thermal stability for NIR pc-LEDs, Chem. Commun. 56 (2020) 4644-4647. https://doi.org/10.1039/d0cc01838d.

[6] J. Qiao, G. Zhou, Y. Zhou, Q. Zhang, Z. Xia, Divalent europium-doped near-infrared-emitting phosphor for light-emitting diodes, Nat. Commun. 10 (2019) 2567. https://doi.org/10.1038/s41467-019-13293-0.

[7] J. Zhang, C. Jin, Structure, Morphology and Upconversion Luminescence of Rare Earth Ions Doped $LiY_9(SiO_4)_6O_2$ for Temperature Sensing, Ind. Eng. Chem. Res. 58 (2019) 3490-3498. https://doi.org/10.1021/acs.iecr.8b05543.

[8] T. Nakanishi, S. Tanabe, Novel Eu^{2+}-activated glass ceramics precipitated with green

and red phosphors for high-power white LED, IEEE J. Sel. Top. Quant. 15 (2009) 1171-1176. https://doi.org/10.1109/JSTQE.2009.2014396.

[9] B. Zheng, X. Zhang, D. Zhang, F. Wang, Z. Zheng, X. Yang, Q. Yang, Y. Song, B. Zou, H. Zou, Ultra-wideband phosphor $Mg_2Gd_8(SiO_4)_6O_2$: Ce^{3+}, Mn^{2+}: Energy transfer and pressure-driven color tuning for potential applications in LEDs and pressure sensors, Chem. Eng. J. 427 (2022) 131897. https://doi.org/10.1016/j.cej.2021.131897.

[10] A.M. Latshaw, G. Morrison, K.D.Z. Loye, A.R. Myers, M.D. Smith, H.C. Zur Loye, Intrinsic blue-white luminescence, luminescence color tunability, synthesis, structure, and polymorphism of $K_3YSi_2O_7$, Cryst. Eng. Comm. 18 (2016) 2294-2302. https://doi.org/10.1039/c6ce00177g.

[11] V.A. Pustovarov, K.V. Ivanovskikh, Y.E. Khatchenko, M. Bettinelli, Q. Shi, Luminescence Spectroscopy and Decay Kinetics of Pr^{3+} Ions in $K_3LuSi_2O_7$: Pr^{3+}, Phys. Solid State. 61 (2019) 752–757. https://doi.org/10.1134/S1063783419050263.

[12] S. Lai, M. Zhao, J. Qiao, M.S. Molokeev, Z.G. Xia, Data-Driven Photoluminescence Tuning in Eu^{2+}-Doped Phosphors, J. Phys. Chem. Lett. 11 (2020) 5680-5685. https://doi.org/10.1021/acs.jpclett.0c01471.

[13] J. Qiao, M. Amachraa, M. Molokeev, Y.C. Chuang, S.P. Ong, Q. Zhang, Z. Xia, Engineering of $K_3YSi_2O_7$ to Tune Photoluminescence with Selected Activators and Site Occupancy, Chem. Mater. 31 (2019) 7770-7778. https://doi.org/10.1021/acs.chemmater.9b02990.

[14] W. Zhou, Z. Sun, J. Luo, X. Zhang, Q. Pang, L. Zhou, Great emission enhancement of high-efficient broadband $K_3YSi_2O_7$: Eu red phosphor *via* enhancing crystallinity, J.

Alloys Compd. 854 (2021) 157188. https://doi.org/10.1016/j.jallcom.2020.157188.

[15] S. Kovač, P.Z. Dabić, A.S. Kremenović, Crystal structure of $K_3EuSi_2O_7$, J. Serb. Chem. Soc. 86 (2021) 663-672. https://doi.org/10.2298/JSC210218026K.

[16] J.D. Napper, R.C. Layland, M.D. Smith, H.-C. Zur Loye, Crystal growth and structure determination of the new silicate $K_3ScSi_2O_7$, J. Chem. Crystallogr. 34, (2004) 347-351. https://doi.org/10.1023/B:JOCC. 0000028666.53348.fc

[17] I. Vidican, M.D. Smith, H.C. Zur Loye, Crystal growth, structure determination, and optical properties of new potassium-rare-earth silicates $K_3RESi_2O_7$ (RE = Gd, Tb, Dy, Ho, Er, Tm, Yb, Lu), J. Solid State Chem. 170 (2003) 203-210. https://doi.org/10.1016/S0022-4596(02)00029-4.

[18] N. Nunotani, Y. Asakawa, M. Watanabe, N. Imanaka, Crystal structure and photoluminescent property of Eu^{3+}-doped $K_3GdSi_2O_7$, J. Asian Ceram. Soc. 5 (2017) 377-380. https://doi.org/10.1016/j.jascer.2017.07.002.

[19] P.Z. Dabić, M.G. Nikolić, S. Kovač, A. Kremenović, Polymorphism and photoluminescence properties of $K_3ErSi_2O_7$, Acta Crystallogr. C Struct. Chem. 75 (2019) 1417-1423. https://doi.org/10.1107/S2053229619011926.

[20] P.S. Solanki, S. Balabhadra, M.F. Reid, V.B. Golovko, J.P.R. Wells, Upconversion Thermometry Using Yb^{3+}/Er^{3+} Co-Doped KY_3F_{10} Nanoparticles, ACS Appl. Nano Mater. 4 (2021) 5696-5706. https://doi.org/10.1021/acsanm.1c00353.

[21] Y. Guo, J. Xie, M. Yu, W. Huang, H. Yang, X. Li, L. Wang, Q. Zhang, The enhanced up-conversion green by Yb-Mn dimer in $NaBiF_4$: $Yb^{3+}/Er^{3+}/Mn^{2+}$ for optical fiber temperature sensor, J. Alloys Compd. 888 (2021) 161497.

https://doi.org/10.1016/j.jallcom.2021.161497.

[22] Y. Mao, P. Xian, L. Jiang, S. Hu, J. Tang, J. Yang, Temperature sensing performance based on up-conversion luminescence in hydrothermally synthesized Yb^{3+}/Er^{3+} co-doped $NaScF_4$ phosphors, Dalton Trans. 49 (2020) 7862-7871. https://doi.org/10.1039/d0dt00809e.

[23] L.J. Li, Y. Tong, J. Chen, Y.H. Chen, G. Abbas Ashraf, L.P. Chen, T. Pang, H. Guo, Up-conversion and temperature sensing properties of $Na_2GdMg_2(VO_4)_3$: Yb^{3+}, Er^{3+} phosphors, J. Am. Ceram. Soc. 105 (2022) 384-391. https://doi.org/10.1111/jace.18070.

[24] Y. Zhang, Y. Cao, Y. Zhao, X. Wang, S. Ran, L. Cao, L. Zhang, B. Chen, Optical temperature sensor based on upconversion luminescence of Er^{3+} doped $GdTaO_4$ phosphors, J. Am. Ceram. Soc. 104 (2021) 361-368. https://doi.org/10.1111/jace.17480.

[25] J. Chen, W.N. Zhang, S.F. Cui, X.S. Peng, F.F. Hu, R.F. Wei, H. Guo, D.X. Huang, Up-conversion luminescence properties and temperature sensing performances of $Ba_5Y_8Zn_4O_{21}$: Yb^{3+}, Er^{3+} phosphors, J. Alloys Compd. 875 (2021) 159922. https://doi.org/10.1016/j.jallcom.2021.159922.

[26] V. Gutiérrez-Cano, F. Rodríguez, J.A. González, R. Valiente, Upconversion and Optical Nanothermometry in $LaGdO_3$: Er^{3+} Nanocrystals in the RT to 900 K Range, J. Phys. Chem. C. 123 (2019) 29818-29828. https://doi.org/10.1021/acs.jpcc.9b06959.

[27] J. Xue, Z. Yu, H.M. Noh, B.R. Lee, B.C. Choi, S.H. Park, J.H. Jeong, P. Du, M. Song, Designing multi-mode optical thermometers *via* the thermochromic $LaNbO_4$: Bi^{3+}/Ln^{3+}

(Ln = Eu, Tb, Dy, Sm) phosphors, Chem. Eng. J. 415 (2021) 128977. https://doi.org/10.1016/j.cej.2021.128977.

[28] J. Zhang, C. Jin, Electronic structure, upconversion luminescence and optical temperature sensing behavior of Yb^{3+}-Er^{3+}/Ho^{3+} doped $NaLaMgWO_6$, J. Alloys Compd. 783 (2019) 84-94. https://doi.org/10.1016/j.jallcom.2018.12.281.

[29] Y. Li, J. Zhang, X. Zhang, Y. Luo, X. Ren, H. Zhao, X. Wang, L. Sun, C. Yan, Near-infrared to visible upconversion in Er^{3+} and Yb^{3+} codoped Lu_2O_3 nanocrystals: Enhanced red color upconversion and three-photon process in green color upconversion, J. Phys. Chem. C. 113 (2009) 4413-4418. https://doi.org/10.1021/jp810275t.

[30] R.D. Shannon, Revised effective ionic radii and systematic studies of interatomie distances in halides and chaleogenides. Acta Cryst. A. 32 (1976) 751-767. https://doi.org/10.1107/S0567739476001551

[31] W.F. Peng, S.Y. Zhou, G.X. Liu, Q.L. Xiao, J.X. Meng, R. Zhang, Combustion synthesis and upconversion luminescence of $CaSc_2O_4$: Yb^{3+}, Er^{3+} nanopowders, J. Rare. Earths. 29 (2011) 330-334. https://doi.org/10.1016/S1002-0721(10)60454-1.

[32] G.F. Wang, W.P. Qin, L.L. Wang, G.D. Wei, P.F. Zhu, D.S. Zhang, F.H. Ding, Synthesis and upconversion luminescence properties of $NaYF_4$: Yb^{3+}/Er^{3+} microspheres, J. Rare. Earths. 27 (2009) 394-397. https://doi.org/10.1016/S1002-0721(08)60258-6.

[33] J. Liao, Z. Han, J. Huang, B. Fu, Y. Sun, H. Yuan, H. Wen, Sol-gel synthesis and optical temperature sensing properties of $PbTiO_3$: Yb^{3+}/Er^{3+} phosphors, J. Phys. Chem. Solids. 162 (2022) 110515. https://doi.org/10.1016/j.jpcs.2021.110515.

[34] J. Zhang, X. Li, G. Chen, Upconversion luminescence of $Ba_9Y_2Si_6O_{24}$: Yb^{3+}-Ln^{3+} (Ln = Er, Ho, and Tm) phosphors for temperature sensing, Mater. Chem. Phys. 206 (2018) 40-47. https://doi.org/10.1016/j.matchemphys.2017.12.007.

[35] W. Liu, X. Wang, Q. Zhu, J.G. Li, Tb^{3+}/Mn^{2+} singly/doubly doped $Sr_3Ce(PO_4)_3$ for multi-color luminescence, excellent thermal stability and high-performance optical thermometry, J. Alloys Compd. 829 (2020) 154563. https://doi.org/10.1016/j.jallcom.2020.154563.

[36] H.A. Klasens, Transfer of energy between centres in zinc sulphide phosphors, Nature. 158 (1946) 306-307. https://doi.org/10.1038/158306c0.

[37] Y. Gao, F. Huang, H. Lin, J.C. Zhou, J. Xu, Y.S. Wang, A Novel Optical Thermometry Strategy Based on Diverse Thermal Response from Two Intervalence Charge Transfer States, Adv. Funct. Mater. 26 (2016) 3139-3145. https://doi.org/10.1002/adfm.201505332.

[38] W. Gao, W. Ge, J. Shi, X. Chen, Y. Li, A novel upconversion optical thermometers derived from non-thermal coupling levels of CaZnOS: Tm/Yb phosphors, J. Solid State Chem. 297 (2021) 122063. https://doi.org/10.1016/j.jssc.2021.122063.

[39] X. Yang, Z. Wu, Z. Yang, X. Zhao, C. Song, M. Yuan, K. Han, H. Wang, S. Li, X. Xu, Flame-made Y_2O_3: Yb^{3+}/Er^{3+} upconversion nanoparticles: Mass production synthesis, multicolor tuning and thermal sensing studies, J. Alloys Compd. 854 (2021) 157078. https://doi.org/10.1016/j.jallcom.2020.157078.

[40] H. Zhang, Y. Liang, H. Yang, S. Liu, H. Li, Y. Gong, Y. Chen, G. Li, Highly Sensitive Dual-Mode Optical Thermometry in Double-Perovskite Oxides *via* Pr^{3+}/Dy^{3+}Energy

Transfer, Inorg. Chem. 59 (2020) 14337-14346. https://doi.org/10.1021/acs.inorgchem.0c02118.

[41] Z. Cao, X. Wei, L. Zhao, Y. Chen, M. Yin, Investigation of SrB_4O_7: Sm^{2+} as a Multimode Temperature Sensor with High Sensitivity, ACS Appl. Mater. Interfaces. 8 (2016) 34546-34551. https://doi.org/10.1021/acsami.6b10917.

[42] M. Wu, D. Deng, F. Ruan, B. Chen, S. Xu, A spatial/temporal dual-mode optical thermometry based on double-sites dependent luminescence of $Li_4SrCa(SiO_4)_2$: Eu^{2+} phosphors with highly sensitive luminescent thermometer, Chem. Eng. J. 396 (2020) 125178. https://doi.org/10.1016/j.cej.2020.125178.

[43] C. Xie, P. Wang, Y. Lin, X. Wei, M. Yin, Y. Chen, Temperature-dependent luminescence of a phosphor mixture of Li_2TiO_3: Mn^{4+} and Y_2O_3: Dy^{3+} for dual-mode optical thermometry, J. Alloys Compd. 821 (2020) 153467. https://doi.org/10.1016/j.jallcom.2019.153467.

[44] J. Wang, R. Lei, S. Zhao, F. Huang, D. Deng, S. Xu, H. Wang, Color tunable Bi^{3+}/Eu^{3+} co-doped La_2ZnTiO_6 double perovskite phosphor for dual-mode ratiometric optical thermometry, J. Alloys Compd. 881 (2021) 160601. https://doi.org/10.1016/j.jallcom.2021.160601.

A novel $K_3(Y_{0.88}Yb_{0.10}Er_{0.02})Si_2O_7$ silicate phosphor for multi-mode thermometry of high sensitivity through up-conversion luminescence

Jiantong Wang,[a] Bowen Wang,[a] Yuhan Teng,[a] Changshuai Gong,[a] Xuyan Xue,[a] Xuejiao Wang,[a*] Ji-Guang Li[b*]

[a]College of Chemistry and Materials Engineering, Bohai University, Jinzhou, Liaoning 121007, China

[b]Research Center for Functional Materials, National Institute for Materials Science, Tsukuba, Ibaraki 305-0044, Japan

*Corresponding author

Dr. Xuejiao Wang
Bohai University
Jianzhou, China
Tel: +86-416-3400708
E-mail: wangxuejiao@bhu.edu.cn

Dr. Ji-Guang Li
National Institute for Materials Science
Ibaraki, Japan
Tel: +81-29-860-4394
E-mail: li.jiguang@nims.go.jp

Abstract

Non-contract optical thermometry shows great advantages for temperature measurement in harsh environments, and it is highly desired to develop novel and high-performance systems. In this work, a novel $K_3(Y_{0.88}Yb_{0.10}Er_{0.02})Si_2O_7$ phosphor was synthesized *via* solid-state reaction, and its up-conversion luminescence and optical thermometric performance were systematically investigated. Under 980 nm excitation, the $K_3(Y_{0.88}Yb_{0.10}Er_{0.02})Si_2O_7$ phosphor showed a strong green UC emission through a three photon process. The phosphor was found well capable of sensing temperature *via* the multi-modes of fluorescence intensity ratio (FIR) of thermally/non-thermally coupled energy levels and fluorescence lifetime (FL). The maximum absolute (S_A) and relative (S_R) sensitivities are $S_A = 156\times10^{-4}$ K^{-1} (I_{531}/I_{555}, 298 K) and $S_R = 1.80\%$ K^{-1} (I_{519}/I_{555}, 298 K) *via* the FIR mode, and are $S_A = 661\times10^{-4}$ K^{-1} (548 K) and $S_R = 9.77\%$ K^{-1} (298 K) *via* the FL mode, which are higher than those of most previous studies.

Keywords: up-conversion; silicate; optical thermometry; rare earth luminescence

1. Introduction

Silicate compounds are an important phosphor family, which have aroused great research interests [1-9]. Phosphors based on silicates have good thermal and chemical stability and are widely used in cathode-ray luminescence and photoluminescence. Silicates include normal silicate, partial silicate, pyrosilicate, and other different systems. By controlling the ratio of chemical reagents and experimental conditions, different silicate phosphors can be obtained, such as $Ba_2La_8(SiO_4)_6O_2$: Eu^{2+} [2], $MgGd_4Si_3O_{13}$: Ce^{3+}, Mn^{2+} [3], $Mg_2Y_2Al_2Si_2O_{12}$: Tb^{3+}, Eu^{3+}, Tm^{3+} [4], $K_3ScSi_2O_7$: Eu^{2+} [5], etc. Silicates are an important choice for luminescence because of their significant absorption of ultraviolet (UV)/near-UV/blue light and low cost. At the same time, silicate-based phosphors have good physical properties, such as oxidation resistance, moisture resistance, and no interaction with the packaging resin [2,4,8,9]. The $[SiO_4]^{4-}$ unit, as the basic building block of silicates, can form relatively complicated crystal structures, which usually contain various complex anionic groups by different joining methods, forming islands, rings, chains, or layered structures [5,6,9]. Among the silicates, $A_3RESi_2O_7$ (A = Na, K; RE = Y, Gd, Lu), especially the $K_3RESi_2O_7$, has aroused intense research interests and various experiments have been carried out for the system [5,6,10-19]. It is found that different emissions, such as near-infrared emission [5,6], white emission [10], and near-ultraviolet emission [11], can be realized by adjusting the RE site.

However, the up-conversion (UC) luminescence of this $K_3RESi_2O_7$ system has not been reported up to date to the best of our knowledge. One of the reasons is that the compound is typically synthesized by the traditional solid-phase method, which, although effective for phosphor selection and synthesis, would produce micron-sized

large particles. It is difficult to obtain phosphors of nanometer size by this method, which greatly limits the application of UC phosphors of this system in the fields of biomarkers and anti-counterfeiting. Another reason is that the research interests of UC system are mainly on fluoride with low phonon energy, which would produce high UC efficiency [20-22]. However, fluoride is toxic, and its toxicity is related to its ability to dissociate fluorine ions.

Recently, the UC phosphors activated by Yb^{3+}-Er^{3+} pair are finding promising application as non-contact thermometers [7,20-23]. The intensity ratio of the 520 nm ($^2H_{11/2}\rightarrow{}^4I_{15/2}$) and 550 nm ($^4S_{3/2}\rightarrow{}^4I_{15/2}$) green luminescence Er^{3+} ion is very sensitive to temperature [24]. The temperature change will cause the obvious change in the ratio of these two branches, and the temperature can be determined by the branch ratio. Such application needs high thermal stability phosphors and doesn't require the phosphor particles to be nanosized. In previous studies, common UC phosphors usually use halogen-containing compounds as substrate [20-22], and Yb^{3+}/Er^{3+} co-doped $NaYF_4$($NaYF_4$: Yb^{3+}/Er^{3+}) is the most common UC material with the highest luminous efficiency. However, halogen-containing compounds need irritating and frequently toxic chemicals in the process of their synthesis. Therefore, various researches have been conducted to explore novel systems using the solid-state method [7,25-27]. In view of the outstanding down-conversion photoluminescence and thermal stability of $K_3YSi_2O_7$-based phosphors [10,13,14], we consider $K_3YSi_2O_7$ to be a promising host for UC luminescence. Thus, the typical ion pair of Yb^{3+}-Er^{3+} was doped into $K_3YSi_2O_7$ in this work, and the resulted phosphor was shown to be capable of multi-mode temperature measurement with high sensitivity through UC luminescence.

2. Experimental section

2.1 Reagents and synthesis

The rare earth sources for the synthesis were oxides (Y_2O_3, Yb_2O_3, Er_2O_3, 99.99% pure) bought from Huizhou Ruier Rare Chemical Hi-Tech Co. Ltd., Huizhou, China. The other reagents of K_2CO_3 (99.9% pure) and SiO_2 (99.99% pure) were purchased from Aladdin Industrial Corporation (Shanghai, China) and were used without further purification. $K_3(Y_{0.88}Yb_{0.10}Er_{0.02})Si_2O_7$ phosphors were synthesized by the conventional high-temperature solid-state method, where the contents of Yb and Er were taken as the optimal values of other UC systems [28,29]. The raw materials were weighed according to stoichiometric ratio, ground in agate mortar with alcohol for 20 minutes, mixed evenly, and then transferred to a corundum crucible. Finally, the mixture was heated at 1350 ℃ in a muffle furnace for 6 h in air, with a heating rate of 5 ℃/min before 800 ℃ and 3 ℃/min for 800-1350 ℃.

2.2 Characterization

The crystalline phases of the samples were identified by an X-ray diffractometer (XRD; Model Ultima IV, Rigaku, Tokyo, Japan) with Cu-K_α (λ = 0.15406 nm) radiation *via* the step-scan mode, with a step size of 0.01° and an accumulation time of 2 s in 2θ = 5-120^o range. Temperature-dependent UC spectra (RT-548 K) were measured using an FLS 1000 fluorospectrophotometer (Edinburgh Instruments Ltd., Herrsching am Ammersee, Britain), using a 980 nm continuous wavelength laser (2 W, Model MDL-III-980-2W-18050833) for excitation and a TAP-02 accessory for temperature control. The fluorescence decay kinetics of the main UC emissions were measured with the lifetime testing unit of the FLS 1000 equipment.

3. Results and discussion

3.1 Synthesis and visible-near-infrared luminescence of $K_3(Y_{0.88}Yb_{0.10}Er_{0.02})Si_2O_7$

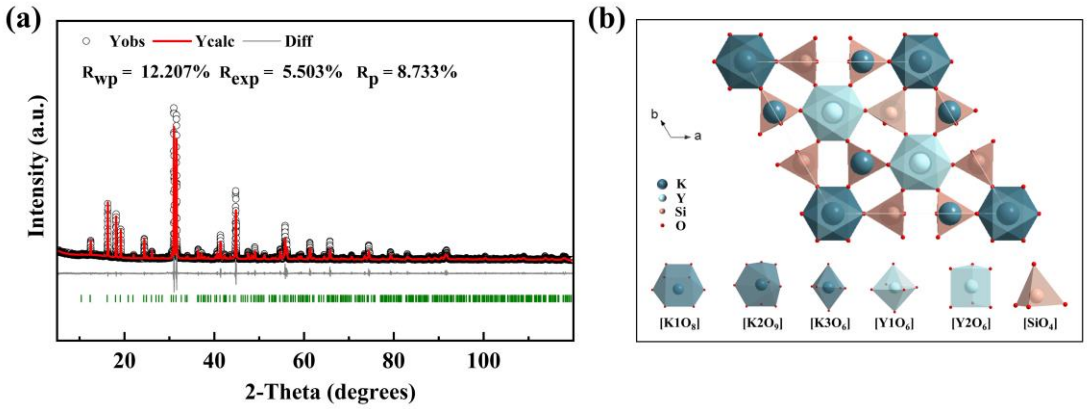

Figure 1 (a) Rietveld refinement for the $K_3(Y_{0.88}Yb_{0.10}Er_{0.02})Si_2O_7$ phosphor, where the observed and calculated patterns, the difference, and the positions of Bragg reflections are in black, red, gray and green, respectively, (b) crystal structure of $K_3YSi_2O_7$, together with the coordination environment of the cation.

Figure 1(a) shows the Rietveld refinement results of the obtained $K_3(Y_{0.88}Yb_{0.10}Er_{0.02})Si_2O_7$ phosphor. The refinement yielded stable results and acceptable reliability factors, which indicate that the product is of high purity. The detailed refinement results are shown in Table 1 and Table 2. According to Loye et al., $K_3YSi_2O_7$ may have two polymorphs, namely $K_3YSi_2O_7$(1) and $K_3YSi_2O_7$(2), which belong to *P*63/*mmc* and *P*63/*mcm* space groups, respectively [10]. In this work, we obtained $K_3YSi_2O_7$(2) with the second space group. Figure 1(b) are the crystal structure observed from the *c*-axis and the coordination polyhedra of cations for $K_3YSi_2O_7$(2). The compound $K_3YSi_2O_7$(2) (ICSD 430538) has a hexagonal structure with lattice constants a = 9.8450 Å, c = 14.3236 Å. c/a = 1.4549. It consists of SiO_4, $K1O_8$, $K2O_9$, $K3O_6$, $Y1O_6$, and $Y2O_6$ units connected by shared oxygen atoms. $K_3YSi_2O_7$(2) has two distinct yttrium sites, one distinct silicon site, three distinct potassium sites, and three distinct oxygen sites [13]. The two yttrium sites are

independent of each other and are located in a hexagonal coordination environment. Y(1) is located in a regular hexagonal octahedron, and Y(2) is located in a hexagonal trigonal prism. $Y1O_6$ is connected to SiO_4 by oxygen atoms at shared vertices, and SiO_4 forms the Si_2O_7 pyrosilicate structure by bridging oxygen atoms at shared vertices. The coordination numbers of K(1), K(2), and K(3) are 8, 9, and 6 respectively. The K(1) site is aligned with Si along the *c*-axis, the K(2) site is aligned with Y(1) along the *c*-axis, and the K(3) site is aligned with Y(2) along the *c*-axis. In addition, it can be seen that the lattice parameters and cell volume of the Yb^{3+}-Er^{3+} co-doped sample is smaller than those of the pure host as also shown in Table S1. This conforms well to the fact that Er^{3+} (R = 0.890, CN = 6) and Yb^{3+} (R = 0.868, CN = 6) have smaller ionic radii than Y^{3+} (R = 0.900, CN = 6) [30], and indicates successful incorporation of the dopant ions to form solid solution.

Table 1 Experimental parameters of powder XRD and refined crystallographic data for $K_3(Y_{0.88}Yb_{0.10}Er_{0.02})Si_2O_7$.

Chemical Formula	$K_3(Y_{0.88}Yb_{0.10}Er_{0.02})Si_2O_7$
Diffractometer	X'Pert Pro, PANalytical
Radiation type	Cu Kα, λ = 1.54060 Å
2θ interval (°)	5.00-120.00
Step size of 2θ (°)	0.01
Space group	*P*63/*mcm* (193)
Z	6
a (Å)	9.8419(2)
b (Å)	9.8419(2)
c (Å)	14.3032(4)
V (Å^3)	1199.85(6)
Number of structure parameters	27
Number of profile parameters	35
[b] R_p (%)	8.73
[c] R_{wp} (%)	12.21
[d] S	2.22

[b] $R_P = \sum |y_i - y_{C,i}| / \sum y_i$; [c] $R_{wp} = \left[\sum w_i |y_i - Y_{C,i}|^2 / \sum w_i y_i^2\right]^{\frac{1}{2}}$; [d] $S = R_{wp} / R_{exp}$

Table 2 Wyckoff positions, atomic coordinates, and occupancies of $K_3(Y_{0.88}Yb_{0.10}Er_{0.02})Si_2O_7$.

Atom	Site	*x*	*y*	*z*	Occupancy
Y1	4	0.3333	0.6667	0	0.89
Yb1	4	0.3333	0.6667	0	0.10
Er1	4	0.3333	0.6667	0	0.01
Y2	2	0	0	0.25	0.91
Yb2	2	0	0	0.25	0.08
Er2	2	0	0	0.25	0.01
K1	12	0.32798	0	0.09211	1
K2	4	0.3333	0.6667	0.25	1
K3	2	0	0	0	1
Si1	12	0.65938	0	0.14315	1
O1	24	0.67437	0.15042	0.09402	1
O2	12	0.81453	0	0.14696	1
O3	6	0.59540	0	0.25	1

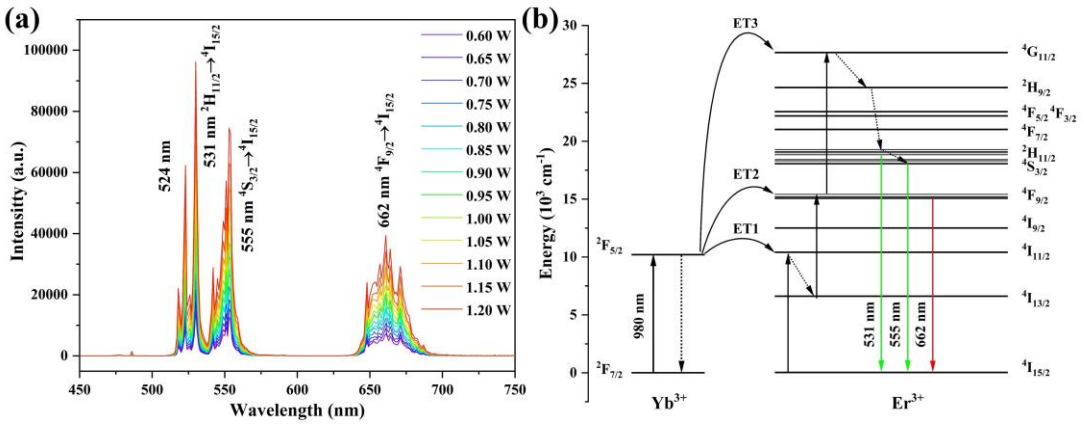

Figure 2 (a) Emission spectra of $K_3(Y_{0.88}Yb_{0.10}Er_{0.02})Si_2O_7$ phosphor in the visible light range (450-750 nm) at different excitation powers of 980 nm laser. (b) The proposed up-conversion mechanism, where ET means energy transfer.

The UC spectra of $K_3(Y_{0.88}Yb_{0.10}Er_{0.02})Si_2O_7$ excited at different powers (0.60-1.20 W) are shown in Figure 2. The emission spectra consist of green emissions in the range of 510-575 nm and red emissions in the 630-700 nm region. The emission peaks at 531 nm and 555 nm belong to the transitions from $^2H_{11/2}$ and $^4S_{3/2}$ excited states to $^4I_{15/2}$ ground state of Er^{3+}, respectively, while the red emission near 670 nm is generated by the transition from $^4F_{9/2}$ to $^4I_{15/2}$. The number of photons (*n*) required to excite the ground state electron to the emission state can be estimated by the $I_{em} \propto P^n$ equation [29]. The logarithmic curves of I_{em} and P^n at different powers are shown in

Figure S1 for the $K_3(Y_{0.88}Yb_{0.10}Er_{0.02})Si_2O_7$ phosphor. The slope of the graph is the number of photons required (*n*). The slope of the curve (*n* value) in Figure S1 is about 3 for green emission and 2 for red emission, indicating that the observed UC luminescence is essentially caused by three (green) and two-photon (red) mechanism. The energy level diagram of Yb^{3+} and Er^{3+} in $K_3(Y_{0.88}Yb_{0.10}Er_{0.02})Si_2O_7$ and the emission mechanism of UC are shown in Figure 2b. The three-photon process corresponding to green emission is as follows. Under the excitation of 980 nm laser, the electrons of Yb^{3+} are excited to the $^2F_{5/2}$ level, from which energy transfer to the neighboring Er^{3+} would take place. The energy absorption of Er^{3+} ion excites electrons from the ground state $^4I_{15/2}$ to the excited state $^4I_{11/2}$ (ET1), followed by non-radiative relaxation (NR) to the $^4I_{13/2}$ level. With the energy of the second excitation photon, the Er^{3+} electrons were raised to the $^4F_{9/2}$ level (ET2). Subsequently, the Er^{3+} electrons were eventually excited to the $^4G_{11/2}$ level by ET3 and then relax to $^2H_{11/2}$ through non-radiative transition. Backing jumping of the $^2H_{11/2}$ electrons to the ground state then produced the green light. The whole process can also be expressed as follows [31,32]:

(1) $^2F_{7/2}$ (Yb^{3+}) + 980 nm photon → $^2F_{5/2}$ (Yb^{3+})

(2) $^2F_{5/2}$ (Yb^{3+}) + $^4I_{15/2}$ (Er^{3+}) → $^2F_{7/2}$ (Yb^{3+}) + $^4I_{11/2}$ (Er^{3+}) (ET1)

(3) $^4I_{11/2}$ (Er^{3+}) → $^4I_{13/2}$ (Er^{3+}) (NR)

(4) $^2F_{5/2}$ (Yb^{3+}) + $^4I_{13/2}$ (Er^{3+}) → $^2F_{7/2}$ (Yb^{3+}) + $^4F_{9/2}$ (Er^{3+}) (ET2)

(5) $^2F_{5/2}$ (Yb^{3+}) + $^4F_{9/2}$ (Er^{3+}) → $^2F_{7/2}$ (Yb^{3+}) + $^4G_{11/2}$ (Er^{3+}) (ET3)

(6) $^4G_{11/2}$ (Er^{3+}) → $^2H_{9/2}$ (Er^{3+}) → $^2H_{11/2}$ (NR)

(7) $^{2}H_{11/2}$ (Er^{3+}) → $^{4}I_{15/2}$ (Er^{3+}) + photons (531 nm)

For the emission peaks at 555 nm, the first six processes are the same as those of the 531 nm emission. The difference is that the electrons at the $^{2}H_{11/2}$ energy level of Er^{3+} relax to the $^{4}S_{3/2}$ by NR, and the occurrence of $^{4}S_{3/2}$ (Er^{3+})→$^{4}I_{15/2}$ (Er^{3+}) and transitions emit photons at 555 nm. For the red emission located at 662 nm, its two-photon process is that, after the first four transition steps, the electron at the $^{4}F_{9/2}$ energy level transits to the ground state and emits a photon.

It can be seen that for $K_3(Y_{0.88}Yb_{0.10}Er_{0.02})Si_2O_7$ phosphor, the increasing excitation power does not change the shape and position of the emission peak, but the intensity of the emission gradually increased.

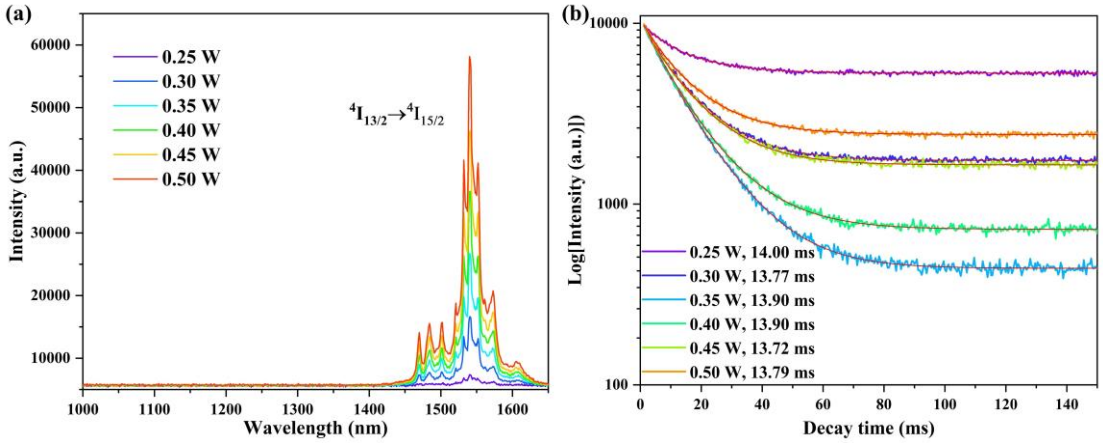

Figure 3 (a) Emission spectra of $K_3(Y_{0.88}Yb_{0.10}Er_{0.02})Si_2O_7$ phosphor in the near-infrared range (1000-1600 nm) at different excitation powers of 980 nm laser. (b) Fluorescence decay kinetics of the 1542 nm emission at different excitation powers (0.25-0.50 W), where the numbers following the power are the average lifetimes.

The emission spectra of $K_3(Y_{0.88}Yb_{0.10}Er_{0.02})Si_2O_7$ in the near-infrared region at different powers are shown in Figure 3a. The strongest peak is at 1542 nm, which corresponds to the $^{4}I_{13/2}$→$^{4}I_{15/2}$ transition of Er^{3+} [33]. It can be seen that the sample has a strong broadband emission in the near-infrared region. The Stark splitting of the NIR emission is evident because of the splitting of the 4*f* level of Er^{3+} ions due to the

action of the crystal field. Figure 3b shows the decay kinetics of the 1542 nm emission, where it was found that all the curves are well fitted using the double-order exponential equation [34,35]:

$$I(t) = A_1 exp(-t/\tau_1) + A_2 exp(-t/\tau_2) \qquad (1)$$

where A_1 and A_2 are constants, t is decay time, I(t) is luminescence intensity at time t, τ_1, and τ_2 are the fast and slow components of lifetime respectively. The average lifetime (τ) can be obtained by the following equation [34,35]:

$$\tau = (A_1\tau_1^2 + A_2\tau_2^2)/(A_1\tau_1 + A_2\tau_2) \qquad (2)$$

The derived τ and A values and the chi-square factor (χ^2) of fittings are summarized in Table S2. The 1542 nm emissions at different powers show similar average lifetime of around 14 ms.

3.2 Multi-mode thermometric properties of $K_3(Y_{0.88}Yb_{0.10}Er_{0.02})Si_2O_7$

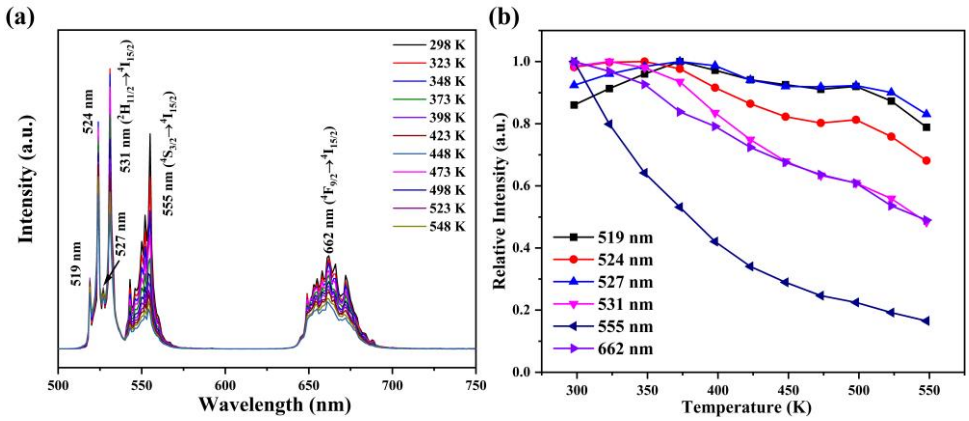

Figure 4 (a) Emission spectra of $K_3(Y_{0.88}Yb_{0.10}Er_{0.02})Si_2O_7$ phosphor excited by 980 nm laser (0.5 W) at different temperatures (RT-548 K). (b) Relative emission intensity for different transitions as a function of the measured temperature.

In practical applications, especially in the field of temperature measurement, the relationship between luminescence intensity and temperature is of great importance. Therefore, we tested the PL spectra of $K_3(Y_{0.88}Yb_{0.10}Er_{0.02})Si_2O_7$ in the temperature range of 298-548 K, as shown in Figure 4a. As can be seen from Figure 4a, the

luminescence intensity of the sample decreases gradually with increasing temperature and the specific CIE coordinates are given in Figure S2 and Table S3. As can be seen from Figure S2, the color coordinates of $K_3(Y_{0.88}Yb_{0.10}Er_{0.02})Si_2O_7$ did not shift much with increasing temperatures. Figure 4b shows the relationship between normalized emission intensity and temperature. The results show that the green emission intensity of 519/527 nm ($^2H_{11/2}\rightarrow{}^4I_{15/2}$) increases with increasing temperature, reaching the maximum value at 373 K and maintaining 97.2% and 98.7% of the maximum intensity at 423 K, respectively. At the highest measurement temperature of 548 K, 78.9% and 83.0% of the maximum emission intensity can still be retained, respectively. For 555 nm ($^4S_{3/2}\rightarrow{}^4I_{15/2}$) emission, the intensity decreases obviously with increasing temperature. The intensity loss rates of $^2H_{11/2}\rightarrow{}^4I_{15/2}$ and $^4S_{3/2}\rightarrow{}^4I_{15/2}$ are different with increasing temperature. This indicates that the prepared phosphor can sense temperature through the fluorescence intensity ratio (FIR) of the thermally coupled $^2H_{11/2}$ and $^4S_{3/2}$ levels and has potential application in the field of optical thermometry. The $^4F_{9/2}\rightarrow{}^4I_{15/2}$ (662 nm) emission also decreased monotonically with increasing temperature. Since $^2H_{11/2}$ and $^4S_{3/2}$ are thermally coupled energy levels (ΔE = 736 cm^{-1}), their population follows Boltzmann distribution. The FIR of the two different green emissions can be expressed as [36,37]:

$$\mathrm{FIR} = \frac{I_H}{I_S} = A \cdot \exp\left(-\frac{\Delta E}{k_B T}\right) + C \qquad (3)$$

where I_H and I_S represent the emission intensity of the $^2H_{11/2}\rightarrow{}^4I_{15/2}$ and $^4S_{3/2}\rightarrow{}^4I_{15/2}$ transitions; ΔE is the energy level gap between corresponding energy levels; k_B is Boltzmann constant; T is the absolute temperature; A and C are constants.

Equation (3) is used to fit the FIR relation with temperature of the two thermal coupled energy levels. The fitting curve is shown in Figure 5a, and the points in the figure are experimental data. It can be seen from the figure that as the temperature rises from 298 K to 548 K, The I_{531}/I_{555} ratios of $K_3(Y_{0.88}Yb_{0.10}Er_{0.02})Si_2O_7$ increase gradually. According to the Boltzmann distribution law, when the temperature increases, electrons are more easily pumped to the higher $^2H_{11/2}$ energy level to reach equilibrium. In addition, the probability of the non-radiative transition from $^4S_{3/2}$ to $^4I_{15/2}$ increases, so the emission at 555 nm is significantly weakened, thus increasing the ratios of I_{531}/I_{555}.

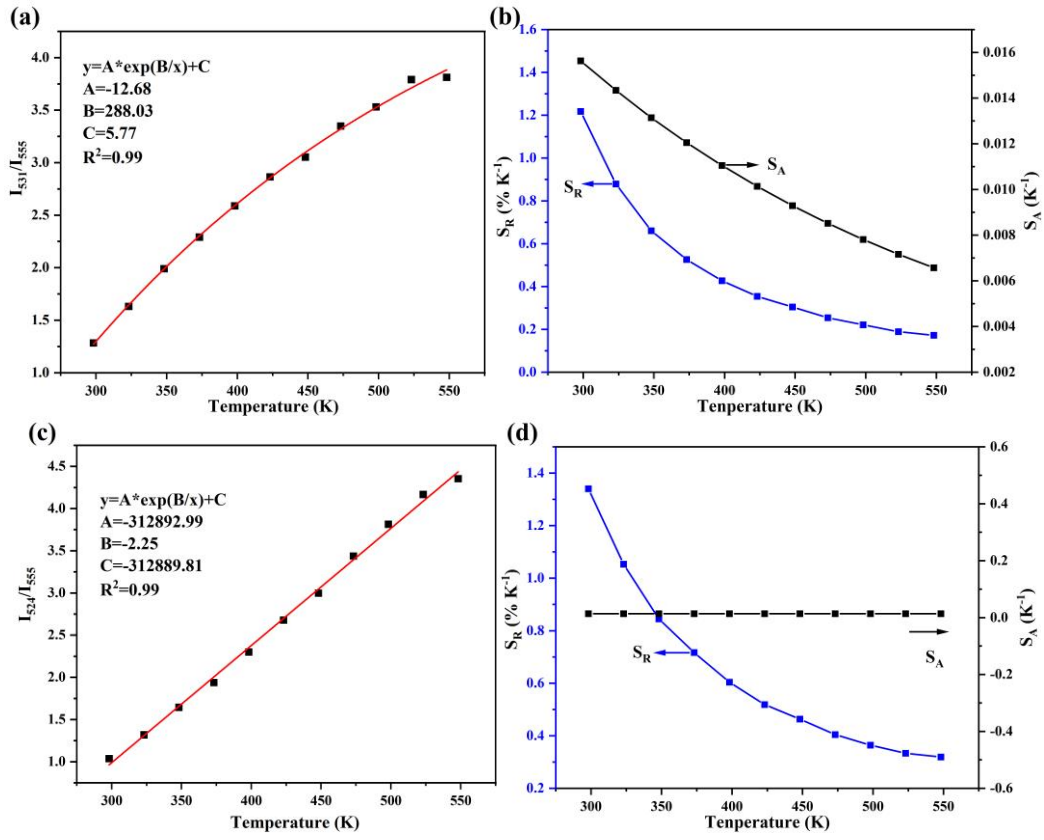

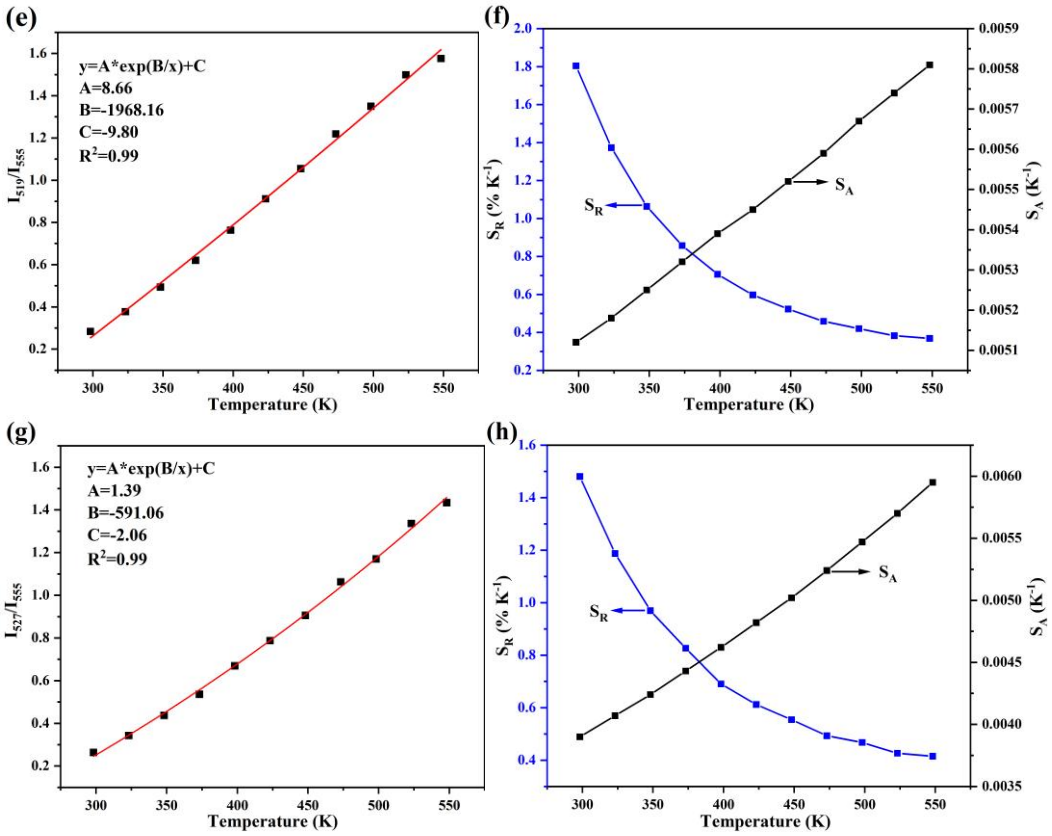

Figure 5 Different FIRs and their corresponding S_A and S_R values as a function of the measurement temperature for the $K_3(Y_{0.88}Yb_{0.10}Er_{0.02})Si_2O_7$ phosphor.

In addition, sensitivity S is an important index to evaluate the sensitivity of phosphors to temperature change, which can be expressed by absolute sensitivity S_A and relative sensitivity S_R. The calculation equations are as follows [37]:

$$S_A = \left|\frac{d(FIR)}{d(T)}\right| = (FIR - C) \times \frac{\Delta E}{k_B T^2} \qquad (4)$$

$$S_R = \left|\frac{d(FIR)}{d(T)}\frac{1}{FIR}\right| = \frac{FIR-C}{FIR} \times \frac{\Delta E}{k_B T^2} \qquad (5)$$

Equation (4) and Equation (5) were used to calculate S_A and S_R, respectively. As shown in Figure 5b, the maximum values of S_A and S_R corresponding to I_{531}/I_{555} are 156×10^{-4} K^{-1}(298 K) and 1.22% K^{-1}(298 K), respectively; while the maximum values of S_A and S_R corresponding to I_{519}/I_{555} are 58×10^{-4} K^{-1}(548 K) and 1.80% K^{-1}(298 K), respectively.

The energy difference (ΔE) of thermally coupled levels is generally between 200 ~ 2000 cm^{-1}. Compared with the traditional technology based on the FIR of thermally

coupled energy levels, the temperature measurement based on non-thermally coupled energy levels (NTCL) is not limited by the energy difference, and the number of energy level pairs is rich, which is beneficial to improve the accuracy of temperature measurement. We calculated the temperature sensitivity of the $K_3(Y_{0.88}Yb_{0.10}Er_{0.02})Si_2O_7$ phosphor. The temperature-dependent FIR of non-thermally coupled energy levels can be fitted by a polynomial function [38]:

$$FIR = \frac{I_{555}}{I_{662}} = A + BT + CT^2 + DT^3 \qquad (6)$$

where A, B, C, and D are constants. As shown in Figure 6a, the variation of the fluorescence intensity ratio FIR(I_{555}/I_{662}) of the non-thermally coupled energy levels with temperature can be well fitted by Equation (6), with R^2 = 0.99. In this case, the sensitivity of temperature sensing can be calculated with the following equation [38]:

$$S = \frac{d(FIR)}{dT} = B + 2CT + 3DT^2 \qquad (7)$$

The curve of sensitivity as a function of temperature is shown in Figure 6b, where the sensitivity reached a maximum value of 157×10^{-4} K^{-1} at 298 K.

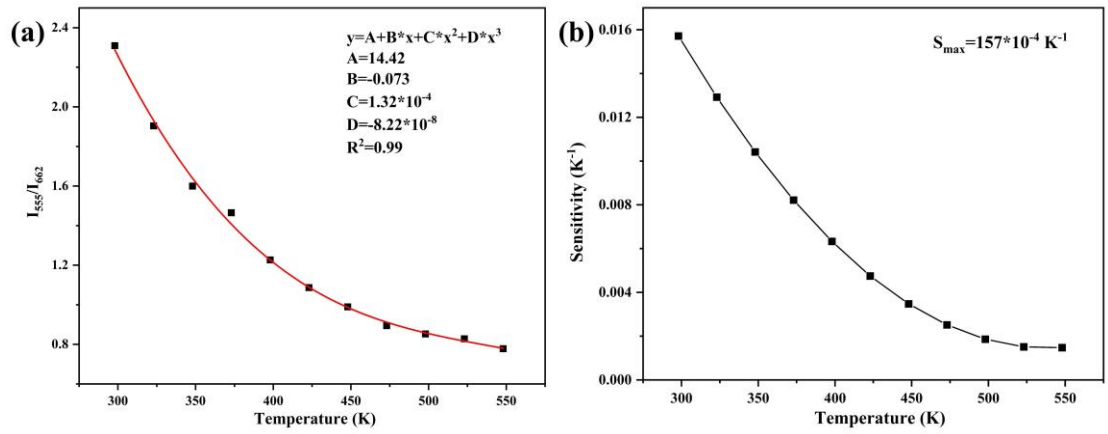

Figure 6 (a) The FIR of the 555 nm and 662 nm emission peaks of $K_3(Y_{0.88}Yb_{0.10}Er_{0.02})Si_2O_7$ as a function of temperature and (b) sensitivity as a function of temperature.

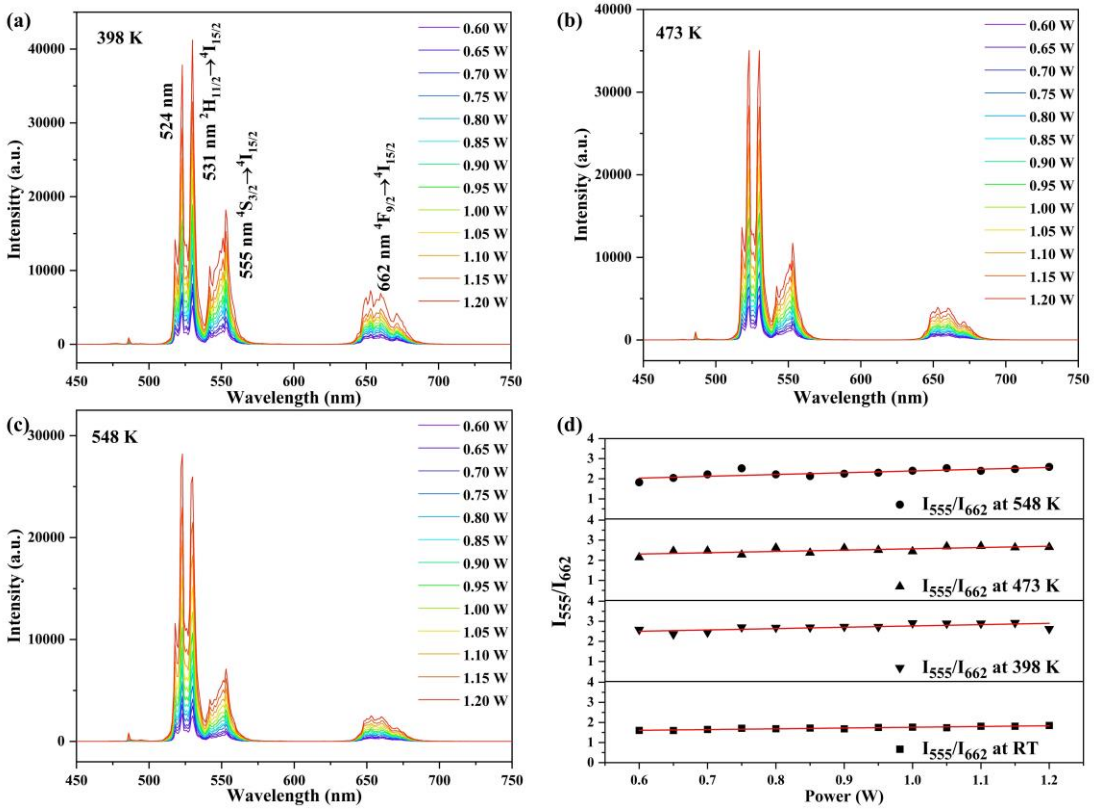

Figure 7 Emission spectra of $K_3(Y_{0.88}Yb_{0.10}Er_{0.02})Si_2O_7$ phosphor excited with different powers 980 nm laser at (a) 398 K, (b) 473 K, and (c) 548 K. (d) The variation trend of I_{555}/I_{662} with excitation power at different temperatures.

Although quite a number of references used Equation (6) for the FIR fitting of non-thermally coupled energy levels, the excitation power was not involved in the equation. Such fitting cannot reflect the influence of the excitation power on FIRs. In order to ensure the accuracy of the results, the power dependent emission spectra at different temperatures (398 K, 473 K, 548 K) were measured and the I_{555}/I_{662} FIR at different excitation powers was evaluated. As seen from the results shown in Figure 7, I_{555}/I_{662} FIR is stable under varying excitation power at different temperatures and, therefore, the influence of excitation power during the temperature-sensing calculation of the non-thermally coupled energy level can be excluded. The influence of excitation power on the other two FIRs were also checked and were shown in Figure S4. It was found that excitation power has a small influence on the FIRs

values.

Table 3 summarizes the S_A and S_R values of several typical phosphors with optical temperature sensing behavior. Through comparison, it was found that the maximum value of S_A and S_R obtained in this work are higher than these of most systems. Among them, the sensitivity values calculated based on non-thermally coupled energy levels are higher than those obtained by the thermally coupled energy levels. The results show that $K_3(Y_{0.88}Yb_{0.10}Er_{0.02})Si_2O_7$ phosphor has potential application value in optical temperature measurement.

Table 3. A summary of S_A and S_R values, and temperature sensing ranges for some typical temperature sensing phosphors.

Ion pair	Mode	Host	Range (K)	$S_A(K^{-1})\times10^{-4}$	$S_R(\%\ K^{-1})$	Ref
Yb^{3+}-Er^{3+}	FIR	KY_3F_{10}(Core-Only)	310-366	-	1.51 (310 K)	[20]
Yb^{3+}-Er^{3+}	FIR	KY_3F_{10}(Core-Shell)	300-365	-	1.24 (316 K)	[20]
$Yb^{3+}/Er^{3+}/Mn^{2+}$	FIR	$NaBiF_4$	298-473	55.9 (473 K)	1.22 (298 K)	[21]
Yb^{3+},Er^{3+}	FIR	$NaScF_4$	298-573	25.6 (548 K)	0.31	[22]
Yb^{3+},Er^{3+}	FIR	$NaScF_4$(EDTA)	298-573	32.8 (548 K)	0.41	[22]
Yb^{3+},Er^{3+}	FIR	$Na_2GdMg_2(VO_4)_3$	303-573	74.9 (479 K)	0.98 (303 K)	[23]
Er^{3+}	FIR	$GdTaO_4$	293-723	41 (475 K)	1.12 (298 K)	[24]
Yb^{3+},Er^{3+}	FIR	$Ba_5Y_8Zn_4O_{21}$	293-563	0.39 (563 K)	136 (293 K)	[25]
Er^{3+}	FIR	$LaGdO_3$	298-873	43 (554 K)	1.20 (298 K)	[26]
Bi^{3+}/Tb^{3+}	FIR	$LaNdO_4$	303-483	410	2.36	[27]
Bi^{3+}/Eu^{3+}	FIR	$LaNdO_4$	303-483	440	1.89	[27]
Bi^{3+}/Dy^{3+}	FIR	$LaNdO_4$	303-483	80	1.26	[27]
Bi^{3+}/Sm^{3+}	FIR	$LaNdO_4$	303-483	310	1.36	[27]
Yb^{3+}/Er^{3+}	FIR	Y_2O_3	323-573	196 (543 K)	-	[39]
Pr^{3+}	FL	La_2MgTiO_6	298-548	2.85	1.81 (473 K)	[40]
Sm^{2+}	FL	$SrBa_4O_7$	298-723	-	3.36 (500 K)	[41]
Eu^{2+}	FL	$Li_4ScCa(SiO_4)_2$	303-573	1470	15.0	[42]
Dy^{3+}/Mn^{4+}	FL	Li_2TiO_3/Y_2O_3	273-373	220 (308 K)	6.67 (339 K)	[43]
Yb^{3+},Er^{3+}	$FIR(I_{531}/I_{555})$	$K_3YSi_2O_7$	298-548	156 (298 K)	1.22 (298 K)	This work
Yb^{3+},Er^{3+}	$FIR(I_{527}/I_{555})$	$K_3YSi_2O_7$	298-548	59 (548 K)	1.48 (298 K)	This work
Yb^{3+},Er^{3+}	$FIR(I_{519}/I_{555})$	$K_3YSi_2O_7$	298-548	58 (548 K)	1.80 (298 K)	This work
Yb^{3+},Er^{3+}	$FIR(I_{524}/I_{555})$	$K_3YSi_2O_7$	298-548	139	1.34 (298 K)	This work
Yb^{3+},Er^{3+}	$FIR_{NTCL}(I_{555}/I_{662})$	$K_3YSi_2O_7$	298-548	157 (298 K)	-	This work
Yb^{3+},Er^{3+}	FL(531 nm)	$K_3YSi_2O_7$	323-548	661 (548 K)	9.77 (298 K)	This work

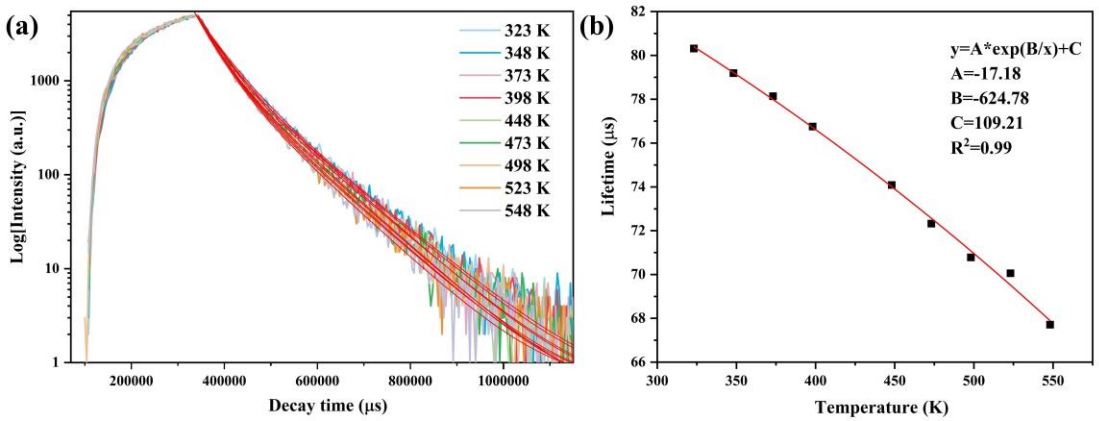

Figure 8 (a) Fluorescence decay kinetics of 531 nm emission at different temperatures (RT-548 K), and (b) the relationship of fluorescence lifetimes for 531 nm emission with measurement temperature (RT-548 K). The intensity in (a) is in logarithmic form.

Figure 8a shows the fluorescence decay curves for the 531 nm emission of $K_3(Y_{0.88}Yb_{0.10}Er_{0.02})Si_2O_7$ phosphor under 980 nm laser excitation at different temperatures. As shown in the figure, all the curves are well fitted using the double-order exponential Equation (1). Then, the average lifetime (τ) can be obtained by the following Equation (2). The derived lifetime of the 531 nm emission is shown in Figure 8b, where it is seen that the lifetime monotonously decreased from 80.31 μs (323 K) to 67.71 μs (548 K). The 531 nm emission at other temperatures showed a similar decay behavior and the derived τ and A values and the chi-square factor (χ^2) of fittings are summarized in Table S4. The χ^2 values for all the fittings are around 1, indicating the high quality of the fitting. It is noteworthy that the fluorescence lifetime of $K_3(Y_{0.88}Yb_{0.10}Er_{0.02})Si_2O_7$ decreases with increasing temperature, which can be attributed to increased non-radiative transitions in the matrix lattice. This trend is the same as that observed from the temperature-dependent emission intensity. As shown in Figure 8b, the lifetime of the 531 nm emission decreases exponentially with increasing temperature T, and can be expressed as τ_{531} = -17.18exp (-624.78/T) + 190.91.

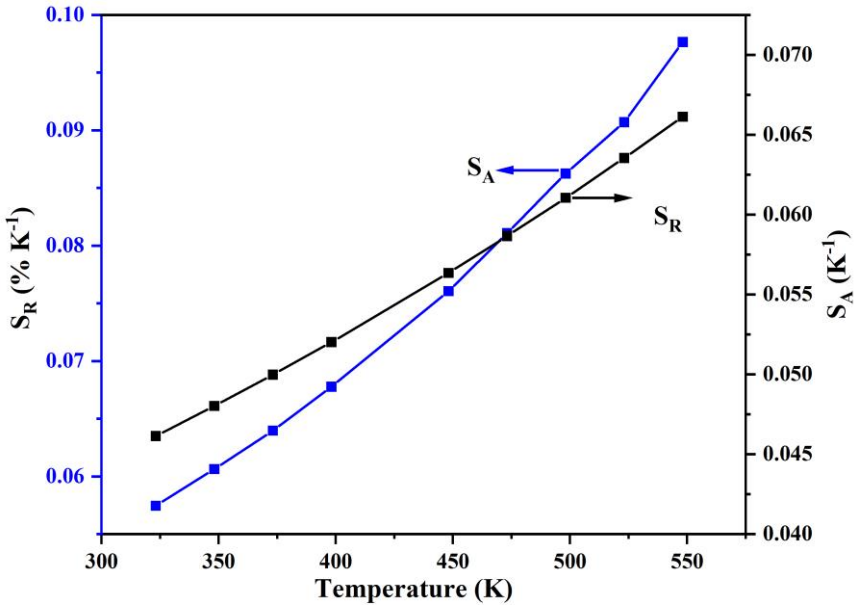

Figure 9 The relative sensitivity S_R and absolute sensitivity S_A based on the fluorescence lifetime of 531 nm emission for $K_3(Y_{0.88}Yb_{0.10}Er_{0.02})Si_2O_7$ phosphor.

Aside from those utilizing the FIR technology, a temperature sensing scheme based on fluorescence lifetime (FL) can also be realized with the thermal quenching characteristics of $K_3(Y_{0.88}Yb_{0.10}Er_{0.02})Si_2O_7$. Similar to the scheme based on FIR, the absolute sensitivity S_A and relative sensitivity S_R of FL based temperature sensing can be calculated by the following Equation [40,42-44]:

$$S_A = \left|\frac{d\tau}{dT}\right| \qquad (8)$$

$$S_R = \frac{1}{\tau}\left|\frac{d\tau}{dT}\right| \qquad (9)$$

As shown in Figure 9, the phosphor has maximum values were 661×10^{-4} K^{-1}(548 K) and 9.77% K^{-1}(548 K) for S_A and S_R, respectively. It can be seen from the figure that S_A and S_R both increase with increasing temperature. By comparing the S_R value based on the FL mode and the S_R value based on the FIR mode, it is obvious that the former is greater than the latter. Nevertheless, as shown in Table 3, the S_R values of both the FIR and FL modes obtained in this work are better than those of most previous studies.

Conclusions

A novel $K_3(Y_{0.88}Yb_{0.10}Er_{0.02})Si_2O_7$ silicate phosphor was prepared by solid reaction. The UC luminescence properties, UC mechanism as well as the performance of optical temperature sensing *via* multi-modes were systematically investigated. The main conclusions are as follows:

(1) The $K_3(Y_{0.88}Yb_{0.10}Er_{0.02})Si_2O_7$ new phosphor exhibits strong green luminescence through $^2H_{11/2}\rightarrow{}^4I_{15/2}$ transition (531 nm) under 980 nm excitation, which occurs through a three photon processes.

(2) $K_3(Y_{0.88}Yb_{0.10}Er_{0.02})Si_2O_7$ is well capable of temperature sensing *via* fluorescence intensity ratio (FIR) with thermally coupled/non-thermally coupled energy levels (TCL/NTCL) and fluorescence lifetime (FL). The maximum S_A and S_R values are $S_A = 156\times10^{-4}$ K^{-1} (I_{531}/I_{555}, 298 K) and $S_R = 1.80\%$ K^{-1} (I_{519}/I_{555}, 298 K) for the FIR mode, and are $S_A = 661\times10^{-4}$ K^{-1} (548 K) and $S_R = 9.77\%$ K^{-1} (298 K) for the FL mode.

Acknowledgements

This work is supported by Natural Science Foundation of Liaoning Province (Grant No. 2020-MS-286). The authors would like to thank Siqi Liu from Shiyanjia Lab (www.shiyanjia.com) for the XRD measurement.

References

[1] X. Ji, J. Zhang, Y. Li, S. Liao, X. Zhang, Z. Yang, Z. Wang, Z. Qiu, W. Zhou, L. Yu, S. Lian, Improving quantum efficiency and thermal stability in blue-emitting $Ba_{2-x}Sr_xSiO_4$: Ce^{3+} phosphor *via* solid solution, Chem. Mater. 30 (2018) 5137-5147.

https://doi.org/10.1021/acs.chemmater.8b01652.

[2] T. Sun, D. Liu, Y.G. Liu, X. Bu, H. Yu, J. Yang, C.A. Xie, J. Chen, A novel cyan-emitting phosphor $Ba_2La_8(SiO_4)_6O_2$: Eu^{2+} for full-spectrum white light-emitting diodes, Opt. Mater. 127 (2022) 1112287. https://doi.org/10.1016/j.optmat.2022.112287.

[3] A. Deng, Z. Wang, X. Zhou, W. Geng, $MgGd_4Si_3O_{13}$: Ce^{3+}, Mn^{2+}: A Dual-Excitation Temperature Sensor, ACS Omega. 7 (2022) 6481-6487. https://doi.org/10.1021/acsomega.1c04710.

[4] X. Huo, Z. Wang, C. Tao, N. Zhang, D. Wang, J. Zhao, Z. Yang, P. Li, Single-component white emitting phosphor $Mg_2Y_2Al_2Si_2O_{12}$: Tb^{3+}, Eu^{3+}, Tm^{3+} for white LEDs, J. Alloys Compd. 902 (2022) 163823. https://doi.org/10.1016/j.jallcom.2022.163823.

[5] Q. Zhang, X. Wang, Z. Tang, Y. Wang, A $K_3ScSi_2O_7$: Eu^{2+} based phosphor with broad-band NIR emission and robust thermal stability for NIR pc-LEDs, Chem. Commun. 56 (2020) 4644-4647. https://doi.org/10.1039/d0cc01838d.

[6] J. Qiao, G. Zhou, Y. Zhou, Q. Zhang, Z. Xia, Divalent europium-doped near-infrared-emitting phosphor for light-emitting diodes, Nat. Commun. 10 (2019) 2567. https://doi.org/10.1038/s41467-019-13293-0.

[7] J. Zhang, C. Jin, Structure, Morphology and Upconversion Luminescence of Rare Earth Ions Doped $LiY_9(SiO_4)_6O_2$ for Temperature Sensing, Ind. Eng. Chem. Res. 58 (2019) 3490-3498. https://doi.org/10.1021/acs.iecr.8b05543.

[8] T. Nakanishi, S. Tanabe, Novel Eu^{2+}-activated glass ceramics precipitated with green

and red phosphors for high-power white LED, IEEE J. Sel. Top. Quant. 15 (2009) 1171-1176. https://doi.org/10.1109/JSTQE.2009.2014396.

[9] B. Zheng, X. Zhang, D. Zhang, F. Wang, Z. Zheng, X. Yang, Q. Yang, Y. Song, B. Zou, H. Zou, Ultra-wideband phosphor $Mg_2Gd_8(SiO_4)_6O_2$: Ce^{3+}, Mn^{2+}: Energy transfer and pressure-driven color tuning for potential applications in LEDs and pressure sensors, Chem. Eng. J. 427 (2022) 131897. https://doi.org/10.1016/j.cej.2021.131897.

[10] A.M. Latshaw, G. Morrison, K.D.Z. Loye, A.R. Myers, M.D. Smith, H.C. Zur Loye, Intrinsic blue-white luminescence, luminescence color tunability, synthesis, structure, and polymorphism of $K_3YSi_2O_7$, Cryst. Eng. Comm. 18 (2016) 2294-2302. https://doi.org/10.1039/c6ce00177g.

[11] V.A. Pustovarov, K.V. Ivanovskikh, Y.E. Khatchenko, M. Bettinelli, Q. Shi, Luminescence Spectroscopy and Decay Kinetics of Pr^{3+} Ions in $K_3LuSi_2O_7$: Pr^{3+}, Phys. Solid State. 61 (2019) 752–757. https://doi.org/10.1134/S1063783419050263.

[12] S. Lai, M. Zhao, J. Qiao, M.S. Molokeev, Z.G. Xia, Data-Driven Photoluminescence Tuning in Eu^{2+}-Doped Phosphors, J. Phys. Chem. Lett. 11 (2020) 5680-5685. https://doi.org/10.1021/acs.jpclett.0c01471.

[13] J. Qiao, M. Amachraa, M. Molokeev, Y.C. Chuang, S.P. Ong, Q. Zhang, Z. Xia, Engineering of $K_3YSi_2O_7$ to Tune Photoluminescence with Selected Activators and Site Occupancy, Chem. Mater. 31 (2019) 7770-7778. https://doi.org/10.1021/acs.chemmater.9b02990.

[14] W. Zhou, Z. Sun, J. Luo, X. Zhang, Q. Pang, L. Zhou, Great emission enhancement of high-efficient broadband $K_3YSi_2O_7$: Eu red phosphor *via* enhancing crystallinity, J.

Alloys Compd. 854 (2021) 157188. https://doi.org/10.1016/j.jallcom.2020.157188.

[15] S. Kovač, P.Z. Dabić, A.S. Kremenović, Crystal structure of $K_3EuSi_2O_7$, J. Serb. Chem. Soc. 86 (2021) 663-672. https://doi.org/10.2298/JSC210218026K.

[16] J.D. Napper, R.C. Layland, M.D. Smith, H.-C. Zur Loye, Crystal growth and structure determination of the new silicate $K_3ScSi_2O_7$, J. Chem. Crystallogr. 34, (2004) 347-351. https://doi.org/10.1023/B:JOCC. 0000028666.53348.fc

[17] I. Vidican, M.D. Smith, H.C. Zur Loye, Crystal growth, structure determination, and optical properties of new potassium-rare-earth silicates $K_3RESi_2O_7$ (RE = Gd, Tb, Dy, Ho, Er, Tm, Yb, Lu), J. Solid State Chem. 170 (2003) 203-210. https://doi.org/10.1016/S0022-4596(02)00029-4.

[18] N. Nunotani, Y. Asakawa, M. Watanabe, N. Imanaka, Crystal structure and photoluminescent property of Eu^{3+}-doped $K_3GdSi_2O_7$, J. Asian Ceram. Soc. 5 (2017) 377-380. https://doi.org/10.1016/j.jascer.2017.07.002.

[19] P.Z. Dabić, M.G. Nikolić, S. Kovač, A. Kremenović, Polymorphism and photoluminescence properties of $K_3ErSi_2O_7$, Acta Crystallogr. C Struct. Chem. 75 (2019) 1417-1423. https://doi.org/10.1107/S2053229619011926.

[20] P.S. Solanki, S. Balabhadra, M.F. Reid, V.B. Golovko, J.P.R. Wells, Upconversion Thermometry Using Yb^{3+}/Er^{3+} Co-Doped KY_3F_{10} Nanoparticles, ACS Appl. Nano Mater. 4 (2021) 5696-5706. https://doi.org/10.1021/acsanm.1c00353.

[21] Y. Guo, J. Xie, M. Yu, W. Huang, H. Yang, X. Li, L. Wang, Q. Zhang, The enhanced up-conversion green by Yb-Mn dimer in $NaBiF_4$: $Yb^{3+}/Er^{3+}/Mn^{2+}$ for optical fiber temperature sensor, J. Alloys Compd. 888 (2021) 161497.

https://doi.org/10.1016/j.jallcom.2021.161497.

[22] Y. Mao, P. Xian, L. Jiang, S. Hu, J. Tang, J. Yang, Temperature sensing performance based on up-conversion luminescence in hydrothermally synthesized Yb^{3+}/Er^{3+} co-doped $NaScF_4$ phosphors, Dalton Trans. 49 (2020) 7862-7871. https://doi.org/10.1039/d0dt00809e.

[23] L.J. Li, Y. Tong, J. Chen, Y.H. Chen, G. Abbas Ashraf, L.P. Chen, T. Pang, H. Guo, Up-conversion and temperature sensing properties of $Na_2GdMg_2(VO_4)_3$: Yb^{3+}, Er^{3+} phosphors, J. Am. Ceram. Soc. 105 (2022) 384-391. https://doi.org/10.1111/jace.18070.

[24] Y. Zhang, Y. Cao, Y. Zhao, X. Wang, S. Ran, L. Cao, L. Zhang, B. Chen, Optical temperature sensor based on upconversion luminescence of Er^{3+} doped $GdTaO_4$ phosphors, J. Am. Ceram. Soc. 104 (2021) 361-368. https://doi.org/10.1111/jace.17480.

[25] J. Chen, W.N. Zhang, S.F. Cui, X.S. Peng, F.F. Hu, R.F. Wei, H. Guo, D.X. Huang, Up-conversion luminescence properties and temperature sensing performances of $Ba_5Y_8Zn_4O_{21}$: Yb^{3+}, Er^{3+} phosphors, J. Alloys Compd. 875 (2021) 159922. https://doi.org/10.1016/j.jallcom.2021.159922.

[26] V. Gutiérrez-Cano, F. Rodríguez, J.A. González, R. Valiente, Upconversion and Optical Nanothermometry in $LaGdO_3$: Er^{3+} Nanocrystals in the RT to 900 K Range, J. Phys. Chem. C. 123 (2019) 29818-29828. https://doi.org/10.1021/acs.jpcc.9b06959.

[27] J. Xue, Z. Yu, H.M. Noh, B.R. Lee, B.C. Choi, S.H. Park, J.H. Jeong, P. Du, M. Song, Designing multi-mode optical thermometers *via* the thermochromic $LaNbO_4$: Bi^{3+}/Ln^{3+}

(Ln = Eu, Tb, Dy, Sm) phosphors, Chem. Eng. J. 415 (2021) 128977. https://doi.org/10.1016/j.cej.2021.128977.

[28] J. Zhang, C. Jin, Electronic structure, upconversion luminescence and optical temperature sensing behavior of Yb^{3+}-Er^{3+}/Ho^{3+} doped $NaLaMgWO_6$, J. Alloys Compd. 783 (2019) 84-94. https://doi.org/10.1016/j.jallcom.2018.12.281.

[29] Y. Li, J. Zhang, X. Zhang, Y. Luo, X. Ren, H. Zhao, X. Wang, L. Sun, C. Yan, Near-infrared to visible upconversion in Er^{3+} and Yb^{3+} codoped Lu_2O_3 nanocrystals: Enhanced red color upconversion and three-photon process in green color upconversion, J. Phys. Chem. C. 113 (2009) 4413-4418. https://doi.org/10.1021/jp810275t.

[30] R.D. Shannon, Revised effective ionic radii and systematic studies of interatomie distances in halides and chaleogenides. Acta Cryst. A. 32 (1976) 751-767. https://doi.org/10.1107/S0567739476001551

[31] W.F. Peng, S.Y. Zhou, G.X. Liu, Q.L. Xiao, J.X. Meng, R. Zhang, Combustion synthesis and upconversion luminescence of $CaSc_2O_4$: Yb^{3+}, Er^{3+} nanopowders, J. Rare. Earths. 29 (2011) 330-334. https://doi.org/10.1016/S1002-0721(10)60454-1.

[32] G.F. Wang, W.P. Qin, L.L. Wang, G.D. Wei, P.F. Zhu, D.S. Zhang, F.H. Ding, Synthesis and upconversion luminescence properties of $NaYF_4$: Yb^{3+}/Er^{3+} microspheres, J. Rare. Earths. 27 (2009) 394-397. https://doi.org/10.1016/S1002-0721(08)60258-6.

[33] J. Liao, Z. Han, J. Huang, B. Fu, Y. Sun, H. Yuan, H. Wen, Sol-gel synthesis and optical temperature sensing properties of $PbTiO_3$: Yb^{3+}/Er^{3+} phosphors, J. Phys. Chem. Solids. 162 (2022) 110515. https://doi.org/10.1016/j.jpcs.2021.110515.

[34] J. Zhang, X. Li, G. Chen, Upconversion luminescence of $Ba_9Y_2Si_6O_{24}$: Yb^{3+}-Ln^{3+} (Ln = Er, Ho, and Tm) phosphors for temperature sensing, Mater. Chem. Phys. 206 (2018) 40-47. https://doi.org/10.1016/j.matchemphys.2017.12.007.

[35] W. Liu, X. Wang, Q. Zhu, J.G. Li, Tb^{3+}/Mn^{2+} singly/doubly doped $Sr_3Ce(PO_4)_3$ for multi-color luminescence, excellent thermal stability and high-performance optical thermometry, J. Alloys Compd. 829 (2020) 154563. https://doi.org/10.1016/j.jallcom.2020.154563.

[36] H.A. Klasens, Transfer of energy between centres in zinc sulphide phosphors, Nature. 158 (1946) 306-307. https://doi.org/10.1038/158306c0.

[37] Y. Gao, F. Huang, H. Lin, J.C. Zhou, J. Xu, Y.S. Wang, A Novel Optical Thermometry Strategy Based on Diverse Thermal Response from Two Intervalence Charge Transfer States, Adv. Funct. Mater. 26 (2016) 3139-3145. https://doi.org/10.1002/adfm.201505332.

[38] W. Gao, W. Ge, J. Shi, X. Chen, Y. Li, A novel upconversion optical thermometers derived from non-thermal coupling levels of CaZnOS: Tm/Yb phosphors, J. Solid State Chem. 297 (2021) 122063. https://doi.org/10.1016/j.jssc.2021.122063.

[39] X. Yang, Z. Wu, Z. Yang, X. Zhao, C. Song, M. Yuan, K. Han, H. Wang, S. Li, X. Xu, Flame-made Y_2O_3: Yb^{3+}/Er^{3+} upconversion nanoparticles: Mass production synthesis, multicolor tuning and thermal sensing studies, J. Alloys Compd. 854 (2021) 157078. https://doi.org/10.1016/j.jallcom.2020.157078.

[40] H. Zhang, Y. Liang, H. Yang, S. Liu, H. Li, Y. Gong, Y. Chen, G. Li, Highly Sensitive Dual-Mode Optical Thermometry in Double-Perovskite Oxides *via* Pr^{3+}/Dy^{3+}Energy

Transfer, Inorg. Chem. 59 (2020) 14337-14346. https://doi.org/10.1021/acs.inorgchem.0c02118.

[41] Z. Cao, X. Wei, L. Zhao, Y. Chen, M. Yin, Investigation of SrB_4O_7: Sm^{2+} as a Multimode Temperature Sensor with High Sensitivity, ACS Appl. Mater. Interfaces. 8 (2016) 34546-34551. https://doi.org/10.1021/acsami.6b10917.

[42] M. Wu, D. Deng, F. Ruan, B. Chen, S. Xu, A spatial/temporal dual-mode optical thermometry based on double-sites dependent luminescence of $Li_4SrCa(SiO_4)_2$: Eu^{2+} phosphors with highly sensitive luminescent thermometer, Chem. Eng. J. 396 (2020) 125178. https://doi.org/10.1016/j.cej.2020.125178.

[43] C. Xie, P. Wang, Y. Lin, X. Wei, M. Yin, Y. Chen, Temperature-dependent luminescence of a phosphor mixture of Li_2TiO_3: Mn^{4+} and Y_2O_3: Dy^{3+} for dual-mode optical thermometry, J. Alloys Compd. 821 (2020) 153467. https://doi.org/10.1016/j.jallcom.2019.153467.

[44] J. Wang, R. Lei, S. Zhao, F. Huang, D. Deng, S. Xu, H. Wang, Color tunable Bi^{3+}/Eu^{3+} co-doped La_2ZnTiO_6 double perovskite phosphor for dual-mode ratiometric optical thermometry, J. Alloys Compd. 881 (2021) 160601. https://doi.org/10.1016/j.jallcom.2021.160601.

cif file

Declaration of interests

☒ The authors declare that they have no known competing financial interests or personal relationships that could have appeared to influence the work reported in this paper.

☐The authors declare the following financial interests/personal relationships which may be considered as potential competing interests: